NTNU – Trondheim
Norwegian University of
Science and Technology

Tribology Mechanisms in Low-Friction Hardbanding Coatings.

Øystein Hurtig Høgsand

Materials Science and Engineering
Submission date: June 2013
Supervisor: Nuria Espallargas, IPM
Co-supervisor: Ragnhild Aune, IMT
Sergio Armada, SINTEF

Norwegian University of Science and Technology
Department of Engineering Design and Materials

Preface and Acknowledgements

This is a master thesis carried out in cooperation between the Department of Material Science and Engineering (IMT) and the Department of Engineering Design and Materials (IPM) at NTNU.
SINTEF has been the supporting scientific partner, and Trio Oiltec Services the industrial partner.

The thesis is a follow-up on full-scale experiments performed during the summer and fall of 2012 by the author (Høgsand [1]). The main objective of the master thesis is to design a small scale tribological lab-setup able to reproduce the wear mechanisms that occur during oil drilling, more specific; the wear mechanisms observed in the full-scale testing. It is of most importance to not only reproduce the wear mechanisms, but to do so by simulating in-field environments. All laboratory experiments and sample preparation were done at NTNU.

I would like to acknowledge my supervisor Professor Nuria Espallargas for her guidance and feedback during the process. I would also like to express my gratitude to Sergio Armada at SINTEF for his inputs and support. I thank Trio Oiltec Services for providing samples.

13.06.2013, Trondheim

Øystein Hurtig Høgsand

Abstract

As the shallow and easily accessible oil and gas reservoirs are becoming depleted, the oil and gas industry has turned its attention towards the deeper and more remote reservoirs. The increased drilling depth, more complex well paths and tougher drilling conditions have pushed the limits of traditional drilling methods. Longer drill strings and increased amount of rotation hours have been found to wear out the well-supporting casing tubes at alarming rates. A measure to deal with these problems have for many years been to apply wear-resistant hardbanding materials on the drill string. Hardbanding materials were in the earlier years developed by trial and error, but now a days full-scale testing is most commonly used. However, full-scale testing is expensive, difficult to control and time consuming. The aim of this master thesis has thus been to design a lab-scale hardbanding/casing wear test setup, able to reproduce already known full-scale wear mechanisms with the use of close-to-field parameters.

A lab-scale pin-on-ring setup were designed and proved able to reproduce many of the wear mechanisms from the full-scale tests. Adhesive wear by galling, which is regarded as the most important wear mechanism with respect to wear rate, was found on many of the casing samples by the presence of work-hardened surface layers. Abrasive wear was most prominent at low contact pressures and at large sand quantities in the system. Fatigue wear, the third mechanism known from full-scale tests, was only present in the most brittle hardbanding samples. It was concluded that the test duration of 15 minutes was too short for this type of wear to evolve.

Sammendrag

Ettersom som de lett tilgjengelige olje og gass reservoarene tømmes, har olje- og gassindustrien rettet oppmerkomheten mot de dypere og mer utilgjengelige reservoarene. Dypere brønner i kombinasjon med mer kompleks brønndesign har utnyttet potensialet til tradisjonelle boremetoder til det fulle. Stadig lengre borestrenger og økning i antall rotasjonstimer har resultert i at foringsrørene i brønnene slites ned urovekkende raskt. I forsøk på å håndtere disse stadig økende problemene har oljeindustrien de siste tiårene benyttet seg av slitasjeresistente lavfriksjonsmaterialer som legges på borestrengens overflate. Disse materialene blir vanligvis referert til som Hardbandingmaterialer. De første hardbandingmaterialene ble utviklet ved prøving og feiling, men idag er det først og fremst fullskala testing som benyttes. Slike tester er imidlertid kostbare, vanskelig å kontrollere og tidkrevende å gjennomføre. Denne masteroppgaven har derfor hatt som mål å konstruere et testoppsett som muliggjør testing av hardbandingmaterialer i labskala. En nødvendig forutsetning for et slikt testoppsett var å reprodusere de samme slitasjemekanismene som finnes i fullskala-tester, men samtidig benytte realistiske testparametere.

Testresultatene viste at mange av slitasjemekanismene fra fullskalaforsøkene også kan reproduseres i labskala. Adhesjon, en av de viktigste slitasjeformene når det kommer til slitasjehastighet, viste seg å ha forekommet på mange av foringsrørprøvestykkene. Dette med signifikant arbeidsherding av de slitte overflatene som grunnlag. Abrasiv slitasje viste seg å være mest fremtredende ved lave kontakttrykk og høy tilsats av sand i systemet. En tredje slitasjemekanisme, utmattingsslitasje, ble observert på bare de to sprøeste hardbandingmaterialene, og da i meget begrenset omfang. Det ble konkludert med at forsøkenes varighet på 15 minutter var for kort tid til at utmatting kunne utvikle seg i tilstrekkelig grad.

Contents

List of Figures

List of Tables

Abbreviations

CoF	-	Coefficient of Friction
EDS	-	Energy Dispersive Spectrometry
ERD	-	Extended Reach Drilling
HB	-	Hardbanding
HRC	-	Hardness Rockwell
HV	-	Hardness Vickers
OWR	-	Oil Water Ratio
PMMA	-	Poly Methyl MethAcrylate
Ra	-	Roughness Average
rpm	-	Rotations Per Minute
Rz	-	Average Maximum Height
SD	-	Sliding Distance
SEM	-	Scanning Electron Microscope
SG	-	Specific Gravity
TE-88	-	Multistation Friction and Wear Tester
TJ	-	Tool joint
WF	-	Wear Factor
WV	-	Wear Volume

1 Introduction

As the shallow and easily accessible oil and gas reservoirs are becoming depleted, the oil and gas industry has turned its attention towards the deeper and more remote reservoirs. The increased drilling depth accompanied by more complex drilling trajectories and multi-branched well designs have pushed the limits of traditional drilling. Longer wells mean longer drill strings and increased number of rotating hours inside the casing tubes, which by itself reduces the lifetime expectancy of the drill stem elements and casings. Moreover, deviations from the originally planned well path, so-called doglegs, along with branching and horizontal drilling are all having a negative impact on the drill stem and casing lifetime.

While drilling of a well is typically planned and managed by the operators, contractors are responsible for the drilling process, which also normally includes supplying the drill pipes. The casing tubes on the other hand are supplied and owned by the operator, since they are cemented in the well and hence not recyclable. This creates some challenges; while the interest of the contractor is to drill efficient with good penetration rates, the operator wants to keep the well integrity as complete as possible, that is, minimal damage to the casing [2].

The solution to this problem has since its first development in the 1970's been to apply a protective metallic coating on the rotating drill string. These coatings are commonly referred to as hardbanding materials and are designed to protect both the drill sting and the casing. While the earliest hardbanding materials successfully protected the drill pipes with the use of wear resistant tungsten carbide particles, they wore out the casing at alarming rates. Since then new, so-called "casing friendly" hardbandings have entered the marked with the ability to increase the lifetime of both drill pipes and casing. Hardbandings are normally applied to the drill pipes with an overlay welding process performed by third party drilling contractors on on-shore locations, such as Trio OilTec Services, located in Stavanger.

The need for continued improvement of the existing- or develop new hardbanding coatings has become stronger as the drilling depths and well complexity have advanced. It was common practice to develop hardbanding materials by trial and error. However, new engineered ways to approach the problems have already yielded coatings specifically designed to the drilling conditions.

Full-scale tests performed during the summer and fall of 2012 by Høgsand [1] found adhesive wear by galling and fatigue wear by spalling to be the main source of wear, but abrasive wear was also present to some extent. The aim of this master thesis is to design a lab-scale test that is able to reproduce these wear mechanisms by the use of close-to field parameters.

2 Background on oil-drilling

2.1 Offshore oil-drilling - An overview

Conventional offshore oil-drilling is an operation in which a pre-planned well path is excavated vertically from the surface located platform down to the reservoir. This is the oldest and simplest way of drilling. The two other main methods are horizontal and slant. Horizontal drilling is a process where the drill path moves in the horizontal direction along the reservoir. Slant drilling is done with an inclined drill path. Modern oil-field well-systems are often designed as a mixture of the three types of trajectories. Many reservoirs can in this way be reached from one platform. Besides from the economical benefits of fewer platforms, the environmental impact is less harmful than the conventional method [3].

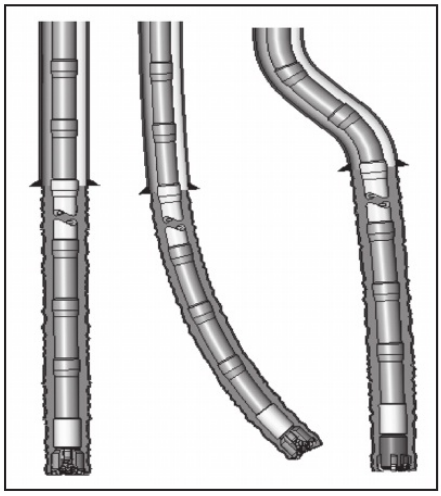

Figure 1: Vertical and directional wells [3].

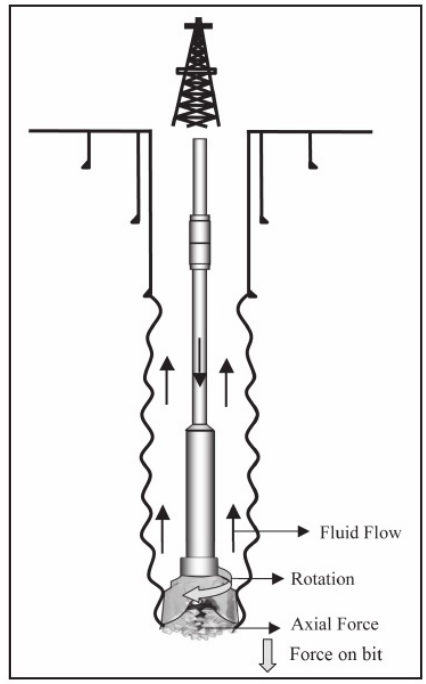

Figure 2: Basic schematic of oil well drilling [3].

A typical well is drilled by the use of a rotating *drill string* with surrounding metal tubing, called *casing*. The top end of the drill string is on the platform deck, while the bottom end is placed on the seabed. Dependent on the type of formation in the seabed, a cutting tool (drill bit) is attached to the bottom end of the string. Rotary motion from the platform at the surface is then transmitted through the drill string to the drill bit, causing the drilling action to occur. In addition, the drill

string conveys drilling fluid to the hole bottom and provides control of borehole direction [3, 4].

In general, drill strings consist of numerous *drill pipes*. Several different types can be chosen dependent on the drilling conditions. The most common type (standard drill pipe), is a cylindrical tubing with a length of 6-12 meters as shown in figure 3. Butt-welded *tool joint* sections are located at both ends of the pipe. These are reinforced by an upset and provide the means for connecting the drill pipes together by integrated screw connections. Each pipe has a pin-end and a box-end, which is the male and female connection-end respectively. As the well-hole is deepened, more drill pipes are attached to the rotating drill string at the platform deck. The drill pipes are designed to withstand the loads that the drilling may induce. Rotating forces against the pipe side-walls, sliding forces, rotating off bottom and dogleg lateral forces amongst the most relevant.

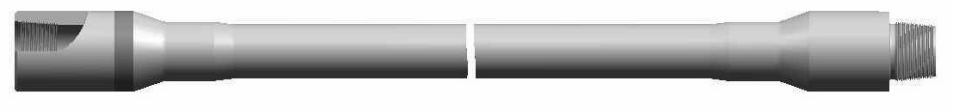

Figure 3: Standard drill pipe. Tool joint box- and pin-end located on the left and right side respectively [5].

As the drill bit is digging deeper into the formation and the drill string is becoming longer by the frequently attached drill pipes, the sand and rock debris needs to be removed from the bore hole. This is done by pumping a fluid called *drilling mud* from the surface to the bottom and back to the surface again, as shown in figure 4. The mud volume is dependent on the hole volume and hole depth, but in general the required volume is high and the mud needs to be reused. A system of mud cleaning devices on the platform deck filter out any settled solids and resets the mud before it is pumped back towards the drill bit where more debris needs to be removed. In addition to removal of drilling debris, the function of the mud includes pressure control and hole stabilization prior to casing/cementing. It also provides cooling and lubrication of the drill string elements, corrosion protection and enhancement in rate of penetration [3, 4].

Before the hydrocarbons can be extracted from the reservoir, the well needs to undergo completion. There are several types of completions, but in general they can be classified as either *open hole* or *cased hole*.

The open hole class represents the simplest type of completions. Wells in this class solely depend on the formation to keep in place and not collapse. These completions have large reservoir contact intervals, allowing for injection or production over larger well sections.

Cased hole completions are made by inserting *casing tubes* in the well bore. Casing tubes are (normally) large diameter carbon steel pipes and exist in different grades and dimensions. The grade is determined by the corrosion and pressure

properties of the well. Computer simulations are therefore always performed in the design stage of a well in order to define the loading conditions that are likely to be encountered, define the mechanical requirements to the casing, and to estimate to what extent the casing will deteriorate through time. The material properties of casings are further described in chapter 4.

Another key factor to casing design is economics. In fact, the cost of casing material can reach up to 20% of the total well cost [6, 7]. Use of high strength casings usually increases the cost, a casing string may therefore consist of several grades.

Cased hole completions are used to prevent burst (internal pressure) or collapse (external pressure) of the borehole and to separate the internal production flow from the surrounding formation. A typical casing string can be thought of as a long telescope tube with the smallest and most extended sections in the deepest parts of the well, as shown in figure 5. The casing pipes are locked in position by filling the gap between the pipes and well bore with cement. A thoroughly planned casing design is of most importance since the smallest casing dictates the production flow and severely restricts the opportunities for further depth extension [3].

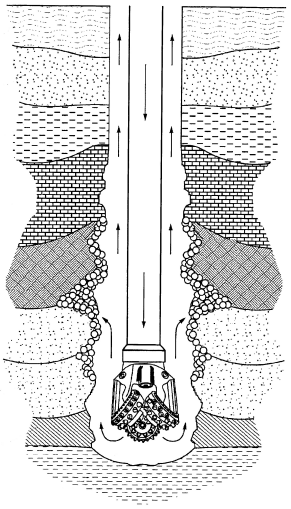

Figure 4: Drilling mud bottom hole flow [8].

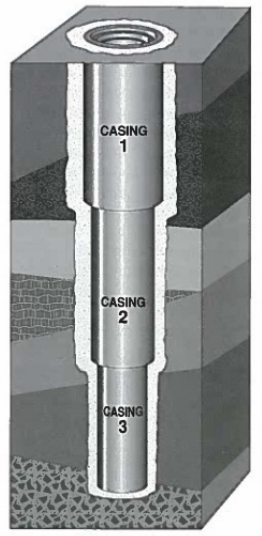

Figure 5: Typical casing design [3].

2.2 Offshore oil-drilling - The challenges

No matter how carefully a drilling operation is planned, some type of problem will most likely occur. Unexpected rock/sand formations, mud leakage, drill pipes getting stuck or casing tubes not fitting properly amongst the common ones [3, p. 355]. In addition to such operational problems, minor issues such as corrosion and wear may accumulate to more serious problems that needs to be dealt with. For the contractors it is important to take care of the drill pipes, which is expensive to replace if damaged. The operators on the other hand need to control the casing integrity in order to prevent potential casing collapse or pressure bursts. Failure on either the drill string or casing, may in the best case scenario result in an expensive halt in the drilling or production process. Worst case would be loss of pressure control that could turn out to be a new DeepWater-Horizon incident [9].

2.2.1 Extended reach drilling and complex wells

As the shallow and easily accessible reservoirs are being depleted and new drilling technologies have been developed, an increased number of wells are drilled with so-called extended reach drilling (ERD). Accompanied by highly deviated drilling trajectories and short radius multi-branched well paths, the number of rotation hours on the drillstring is reaching its limits. Operators have experienced unacceptable levels of wear on the casings, compromising the integrity of the well. Contractors on the other hand have noticed increased wear on the drill pipes, and especially on the tool joint sections [10].

Dogleg is the common-name for particularly crooked sections of the well where the trajectory changes rapidly. While doglegs may be incorporated in the well design, the term most often refers to an unexpected change in direction that occurs faster than expected. Dogleg severity is measured and calculated in degrees per 100 feet (30 meter) of wellbore length. The negative effects associated with doglegs are many. First, the drill bit may not be located at the originally planned position. Secondly, the rapid change in well curvature may become a problem if the preplanned casing string no longer fit the borehole. Further problems are created when drilling is resumed and the drill string passes through the dogleg. As illustrated in figure 6, the forces acting on the drillstring clearly change through the different dogleg sections. With respect to casing wear, the tangent-section is recognized to be the most critical (spot B in figure 6). In this section, the inner casing wall may wear unusually rapid due to the increased drill sting tension and contact forces between tool joints and casing [11]. In addition to compromised mechanical support and potential leakage of drilling fluids, so-called *key-seats* may be created if the drillstring is allowed to wear through the casing. Key-seats, shown in figure 7, are one of the main reasons for large diameter drilling tools getting stuck [12].

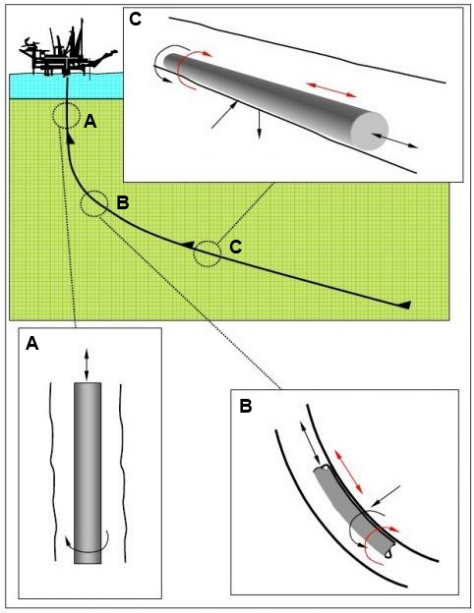

Figure 6: Drill string forces in different sections of a dogleg [13].

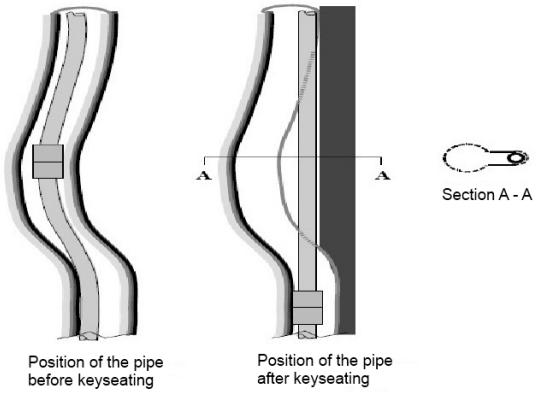

Figure 7: Key-seating [14].

Horizontal drilling or *directional drilling* is a type of drilling were the drill bit is directed towards a specific location outside of the vertical axis. Directional drilling often utilizes special bottom hole assembly components and drill bits that can be steered from the surface. In contrast to vertical wells (section A in figure 6), the force of gravity constricts the drill sting movement to the lowest located area in the directional borehole (section C in figure 6). Cased hole completions of this kind may experience increased wear along the bottom axis of the casing tube [15].

The common feature for all the problem-causing well sections is that when the drill pipes passes through these areas, factors like torque, drag, stick-slip, rotation speed and vibrations worsen the conditions for the drill pipes and casings. Through extensive monitoring and logging of tool joint and casing wear, the application of low-friction metallic coatings on the tool joints (grey section in figure 8) have been recognized as an important measure to control and reduce the problems [2, 10]. These low-friction materials are commonly referred to as Hardfacing or Hardbanding materials.

Figure 8: Hardbanding on tool joint [16].

3 Hardbanding

3.1 History

Hardbanding materials were first developed in the late 1930's by Hughes Tool Company as a solution to the rapid wear on drill pipes when drilling in open hole conditions. First generation hardbandings were applied by welding of a soft steel wire onto the tool joints while simultaneously dropping tungsten particles into the molten weld pool. The result, shown in figure 9, was an extremely hard coating that significantly prolonged the lifetime of the drill pipes by protecting them from wearing out [17].

Figure 9: Raised hardbanding with coarse tungsten particles [18].

However, as the wells became deeper and trajectories more complex the need for cased-hole well sections increased. The so far successful tungsten hardbandings now turned out to wear through the casing wall at alarming rates during drilling operations. Many different particle shapes and sizes were tried out in order to combat this problem, but with no success [10].

A solution was developed by Hughes Tool Company with a tungsten-based hardbanding that was flush-mounted into the tool joints, i.e level with the tool joint material. But again, as the drilling technology evolved and the wells became deeper and more complex, the damage on the casing reached unbearable levels. Back on the drawing board, Hughes came out with an improved version of the flush-mounted hardbanding. Still being flush with the tool joint material, the hardbanding material now consisted of two layers built on top of each other. The upper layer was a mild steel, with the second still tungsten carbides. The idea was

to hinder contact between the tungsten and casing wall. This worked well until the mild steel was worn out and the tungsten/casing contact once again was a fact. Operators realising the complete failure of the hardbandings with respect to casing wear decided to abandon the use of it, and started using drill pipes without hardbanding on the tool joints. What was soon to be realised, was that the naked tool joints caused at least the same amount of wear on the casing than the tungsten carbide hardbanding did. In addition, the contractor noticed that their, now unprotected, drill pipes wore out in no time, which required frequent replacement and repairing, which bill ultimately ended up on the operators' budget.

Early in the 1990's the first "casing friendly hardbanding" was developed by Amorphous Technology Inc. The alloy was chromium based and showed a very low coefficient of friction (CoF), and therefore created very little casing wear. Since the saving of the casing was of utmost importance, little attention was paid to the tool joint wear, and the problem was still only half solved.
However, the new chromium based alloy design created a foundation for further development and there are now many different hardbanding materials on the market (examples in table 1). Still, very few have the ability to fully protect both the casing and the drill pipe simultaneously [6, 10, 17, 19].

Table 1: Some recognized hardbanding materials and their properties [20, 21].

Product	**Producer**	**Wear behaviour**
300XT	Arnco	Open hole wear resistance from abrasion
Tuboscope TC	NOV	Casing friendly
AS-751	Durmat	Extremely high wear resistance from abrasion.
OTW-13CF	Castolin	Casing friendly

3.2 Hardbanding material properties

Casing friendly hardbanding materials entered the market as a result of better testing procedures and systematic alloy design. Typically they consist of a softer base material, with uniformly distributed harder particles. Their composition, as well as mechanical and metallurgical properties, are selected to suit the demands of specific well conditions. The variety of hardbanding materials makes it possible for the drilling contractors to meet the demands of preserving the casing integrity in cased hole conditions, and at the same time protect the drill pipes in open hole drilling.

Hardbanding materials are normally applied to the tool joint by a Gas Metal Arc Welding (GMAW) process (typical parameters are given in appendix A). Welding processes in general can be quite troublesome since the solidification of the weld pool often result in some amount of less favourable microstructural phases. This has become problematic in some hardbanding alloys, which has experienced extensive cracking during welding.

In order to reduce casing wear, several aspects of the hardbanding materials need to be taken into account. Adhesion to the tool joint is obviously of great importance. This is connected to the weldability of the hardbanding material, as well as the compatibility between the tool joint and the hardbanding (similar materials are easier to weld together). On the surface, it needs to be wear resistant, but at the same time be able to minimize casing wear. The many parameters, both mechanical and metallurgical, affect the casing and hardbanding wear in different ways.

3.2.1 Microstructure

Modern hardbanding materials typically consist of a softer base material (matrix), with uniformly distributed harder particles as shown in figure 10. Normally the matrix is either a martensitic tool steel deposit, including some retained austenite, or Fe-base with additions of chromium, carbon, nickel or other alloying elements [2, 22].

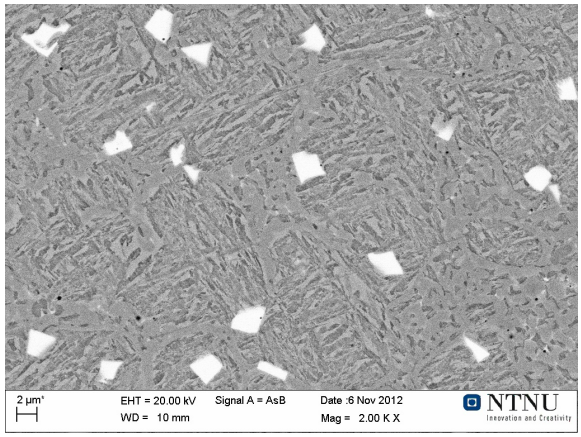

Figure 10: Hardbanding microstructure. Here represented by niobium particles (bright spots) in a martensitic steel matrix [1].

Recently, experiments by Truhan et al. (2007) [23] evaluating various hardbanding materials by the use of the block-on-ring test observed an interesting connection between microstructure and wear rate. Hardbanding materials with a finer, more uniform grain size, and a uniform distribution of carbides showed better friction and wear performance than the more heterogeneous hardbandings. This was opposite to results from pin-on-disk experiments, also done by Truhan et al. in 2005 [22], where the fine grained materials had a higher coefficient of friction than the coarser microstructures. In retrospect, Truhan et al. [23] explains the contrast in results by the difficulties of creating consistent reliable results by using the pin-on-disk test with mud-lubrication.

Harder particles are added to the matrix material in most of the hardbandings. The alloying philosophy vary amongst the different brands names and which kind of wear-behaviour the hardbanding is meant to exhibit. Most common are particles based on either; titanium, chromium, niobium, nickel, molybdenum or boron. The particles are normally added to the weld pool during the application process, where the size and shape is predefined [2].

3.2.2 Mechanical properties

Hardness is one important mechanical property with respect to wear. As will be described in chapter 5, achieving sufficient weld hardness is necessary to obtain the desired tool joint and casing wear resistance. Typical hardness values for hardbanding materials are in the range 600-800 HV.

While hardness affects the wear behaviour of the hardbanding, toughness is important for the integrity of the hardbanding. In general, materials can be categorized into two main groups: High toughness/Low strength and High strength/Low toughness. The materials in the former group have typically great resistance against impact, but low hardness. The latter group has typically high hardness, but are more brittle.

Hardbanding materials need to balance the two extremes. If the hardness is too high, the material becomes brittle and cracking may occur when load is applied. Some alloys are "designed" to crack, but the industry seems to move towards so-called "crack-free" hardbandings. In addition to easier reapplication of hardbanding material, smoother hardbanding surfaces have been found to wear out the casing slower than rougher hardbanding surfaces [24].

It should also be noted that if the hardbanding is too soft, it will wear out in less time, leaving the tool joint exposed. New hardbanding materials are designed to harness the best properties from both categories, high toughness and high strength [2].

4 Casing

As previously mentioned, casing pipes are usually manufactured from plain carbon steel that is heat treated to obtain desired strength. They may however also be made of stainless steel, aluminium, titanium and other materials [25]. Within the steel types, the microstructure normally consists of martensite with some retained austenite.

Most oilfields use casing of the same type, and the only differences are found in the heat treatment. A grading system for standardised strengths of casing is therefore extensively used in the industry, commonly referred to as "casing grade". The appropriate grade for any type of well is based on pressure and corrosion requirements. High strength grades are more expensive than low strength grades. A casing string may thus include several different grades to optimize the cost and at the same time maintain adequate mechanical performance over the total string length. Another important aspect to mention is that, in general, casings with higher yield strength have increased susceptibility to sulfide stress cracking, and the well designer may need to sacrifice strength to ensure prevention of corrosion [7].

Examples of common casing grades and their mechanical properties are listed in table 2 below.

Table 2: Common casing grades and their properties [26, 27].

Casing grade	Yield strength (min MPa)	Tensile strength (MPa)
K-55	420	720
N-80	710	810
P-110	760	960

5 What really wears out the hardbanding/casing?

Ever since the first tungsten carbide hardbanding was introduced in the late 1930's, many questions have been asked about the real effect of hardbanding materials. Are they simply a barrier layer between two more valuable surfaces? Or do they contribute in a more sophisticated way by altering the wear conditions to the better?

Numerous of research projects have tried to find the answers to such questions. While some have led to the development of new hardbanding materials, others have improved the drilling muds. However, the overall complexity of the hardbanding/casing/mud-system, in addition to the empirical nature of wear, makes generalisation of the results very difficult. Still, some findings and conclusions have been found to be consistent and independent on experimental conditions, which will be described after a short introduction to wear mechanisms.

5.1 Wear mechanisms

Wear can be defined as loss of material from a solid surface due to mechanical interaction with another surface [28, 29]. The definition does not include material loss due to corrosion or reduction in dimension when plastic deformation occurs. Such parameters can be included by separate calculations if needed. It should however be mentioned that the combined mechanisms of wear and corrosion (tribocorrosion) cannot simply be estimated as the sum of the two. This would in case be a serious underestimation.

Despite the numerous research projects and casing wear tests that have been carried out, published literature on the subject of wear mechanisms in the hardbanding/casing system isn't abundant. Results and wear mechanisms observed in experiments with tungsten-carbide hardbandings became less important when the new and "casing friendly" hardbanding materials entered the market in the early 1990's. However, recent experiments by Truhan et al. [22, 23] and Doering et al. [30] have identified the following mechanisms to be the main cause of casing/hardbanding wear;

- Adhesive wear
- Abrasive wear
- Fatigue wear

Like most tribological systems, the different types of wear are seldom present in their pure form, but rather as a combination with one predominant type. This is also expected in-field, where the three types may be present at once, but in different parts of the well.

5.1.1 Adhesive wear

Adhesive wear can be described as material transfer between two solid bodies due to some extent of adhesion. In metals, frictional energy is thought to create microwelds when two surfaces are in contact. Similar microstructures and thermal properties promote the adhesion, and self-mated surfaces are thus especially prone to adhesive wear. The mechanisms of transfer can be explained by attractive forces between the surfaces. These forces are thought to act in such a way that they pull fragments of material from one of the surfaces, and sticks to the other. Once a fragment is pulled from its original position, an adhesive wear particle is made.

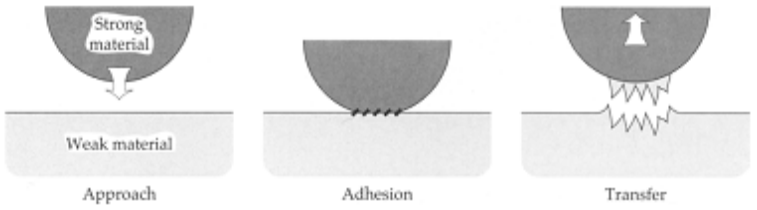

Figure 11: Mechanism of metal transfer due to adhesion. Figure from Stachowiak et.al [29].

Adhesive transfer of material between a softer and a harder material occurs in both directions. In most systems however, fragments from the softer material tend to outnumber the ones from the harder material. These soft fragments also tend to be the largest, thus the net transfer of material is in the "favour" of the harder material. The presence of fragments from the harder material indicate that it contains areas with low strength, and under certain alignments of the two sliding surfaces, these areas may hence produce fragments, which characteristic is the small size [28].

Galling is the common name of severe adhesive wear, characterised by macroscopic, usually localised, roughening of the surface [31]. It occurs mainly in unlubricated low-speed sliding contacts, causing transfer and/or displacement of large fragments of material [32, p. 77-78].

Associated with galling one often find heavily deformed subsurface regions, especially in the softer body. As shown in figure 12, three different zones can usually be identified. Zone 1 represents the bulk of the material where the microstructure is unaffected of the sliding forces at the surface. Moving closer to the surface, the shear strains gradually increases and the microstructure orient itself as if its dragged by the force of sliding. A lamellar-like structure is often seen in the upper parts of this region. Theory suggests that the sliding occurs along the slip-directions of the microstructure. Zone 2 is gradually mixed into zone 3 which can be observed as a really fined grained region. Along with the deformed original microstructure one often find oxides, debris and particles from the counterpart body in this zone [32, p.102-3].

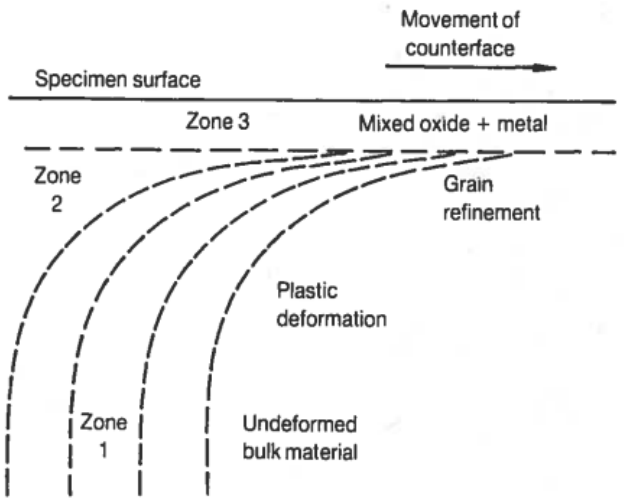

Figure 12: Schematic view of the three different zones of plastic deformation in severely worn metals. Figure from Hutchings [32].

This kind of deformed sub-surface layers were also observed by Doering et al. [30] in samples from in-field, full-scale and lab-scale conditions. The tool joints in these experiments showed extensive cracking/checking on the surface, mainly oriented perpendicular to the sliding direction. Closer examination of the cross sections, shown in figure 13, revealed significant layers of deformation, in which the vertical displacement was greater than the depth. The hardness of the deformed layer was generally 300 HV higher than the bulk material.

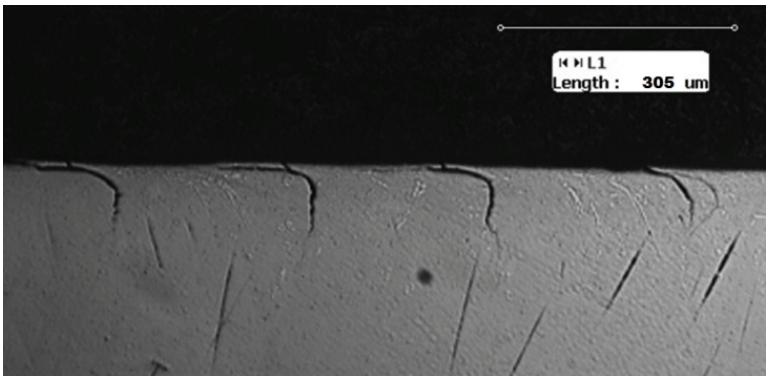

Figure 13: Plastically deformed (work-hardened) sub-surface layers of chrome white iron tool joint tested in DEA-42 full-scale wear tester [30].

In the casing samples from the same experiments (figure14), Doering observed far more plastic flow of material and ridge formation than in the hardbanding counterparts. The worn surfaces almost solely displayed severe adhesive wear, and distinct work-hardened layers were present in both full-scale and lab-scale samples (field worn casing samples are seldom retrieved from the well and thus not examined by Doering et al.).

The main differences between full-scale and lab-scale samples were the depth and distance of material displacement, which were somewhat smaller for the lab-scale samples.

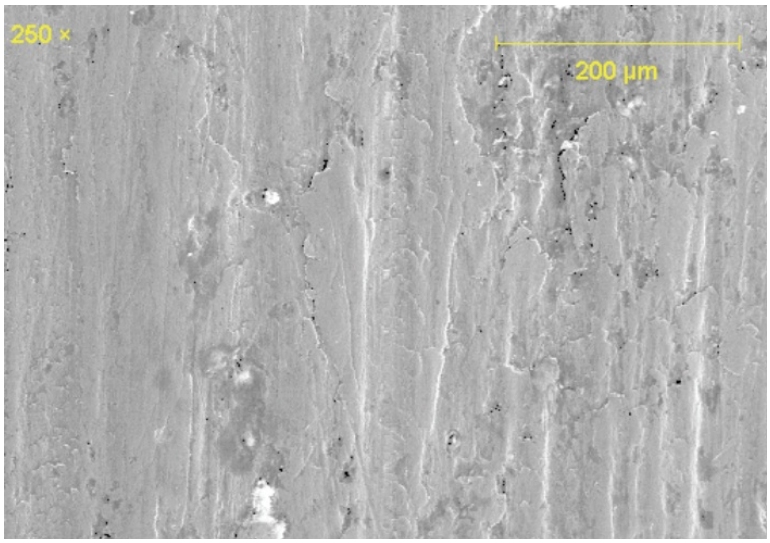

Figure 14: Surface of L-80 casing tested by Doering et al. [30] in a DEA-42 full-scale wear tester. Solely adhesive wear.

5.1.2 Abrasive wear

Abrasive wear occurs when a solid surface is loaded against particles of equal or greater hardness. The particles may enter the system from the surroundings, or created in the adhesive wear regime of the wear system. Abrasive mechanisms are in general more complex than adhesive. It is therefore common to divide abrasive wear into two main modes: *Two body mode* and *Three body mode*. (See figure 15)

Two body abrasion occurs when hard particles are fixed to one of the surfaces, usually the softer one. When the surfaces move relative to each other, the fixed particle may damage the opposing surface (usually the harder one) [29, 33]. In the case of three body abrasion, the particles are *not* fixed to either of the surfaces, but may move around inside the contact making randomly located pits/craters. Experiments have shown that two body wear has approximately 10 times higher

wear rate than three body wear. It has been found that the latter has to compete with other mechanisms such as adhesive wear.

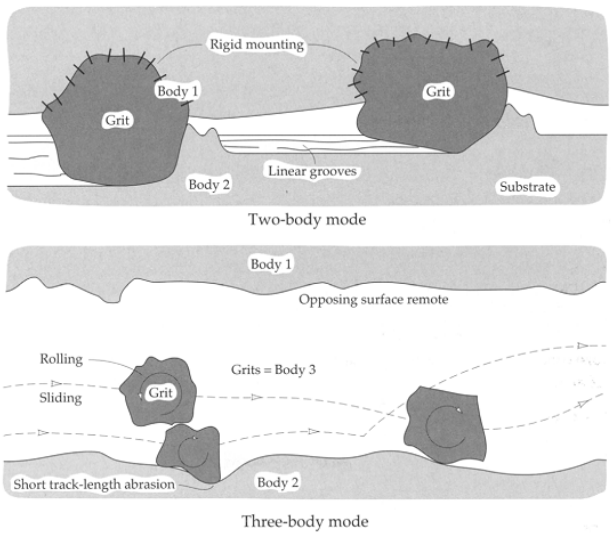

Figure 15: Two and three-body modes of abrasive wear [29, p. 505].

Abrasive removal of material may occur in several ways. In the case of the hardbanding/casing system, separate experiments by Truhan, Best and Doering [18, 23, 30] have identified cutting and ploughing as the most predominant ones (figure 17).

Cutting is the process where a sharp grit cuts the softer surface. The cut material is subsequently removed as wear debris, leaving a nick or scratch on the worn surface (figure 16a).

Ploughing occurs in ductile materials and when a grit is too blunt to cut the surface. Instead, the abraded material is being shoved by the grit. Repeated ploughing may ultimately cause fatigue, thus also the formation of wear debris (figure 16b).

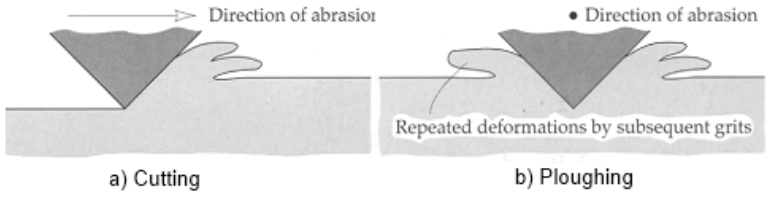

Figure 16: Two-body abrasive wear mechanisms [29].

Cutting or ploughing occurs only when sufficient load is applied and when particles or agglomerates are aligned advantageously to create a nick or scratch in the opposing surface. Both two- and three-body modes may be present, especially if the softer surface is so ductile that the abrading particles become momentarily embedded [23].

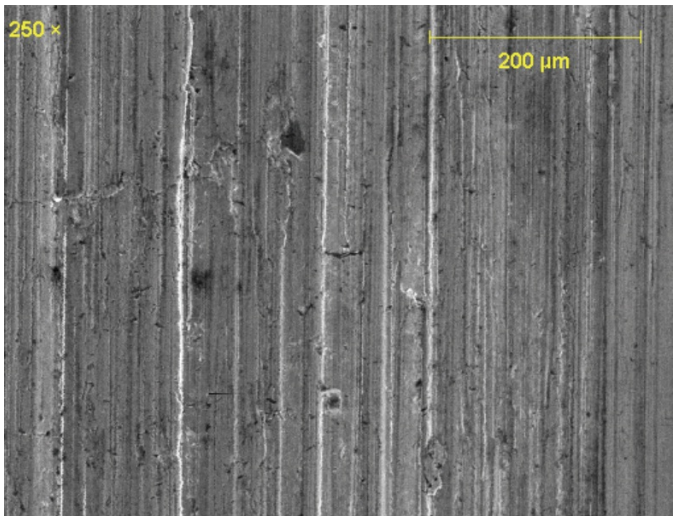

Figure 17: Abrasive grooving and ridge formation by ploughing on hardbanding wear surface tested in lab-scale by Doering et al. [30].

When two materials of different hardness slide against each other, it can always be questioned to what extent the harder material wears the softer. Theory suggest a direct correspondence between wear rate of the softer material (casing) and the relative hardness of the two moving surfaces (tool joint and casing) [29, p. 512-513]. However, block-on-ring experiments by Truhan et al. [23] found no evident correlations between hardbanding hardness, tool joint weight loss and casing weight loss, in spite of the wide variety of hardbanding materials tested (40-66 HRC). This is in accordance with earlier experiments by Erlikh et al. [34] that showed that the hardness of the casing does not greatly affect its wear resistance. Truhan [23] points out that the presence of sand particles in the slurry, which hardness exceeds both hardbanding and casing hardness by far, may cause wear in both surfaces.

5.1.3 Fatigue wear

A third mechanism of wear observed [30] in the hardbanding/casing system is fatigue wear. This form of wear occurs when very high local stresses are repeated a large number of times in the course of sliding or rolling [29, p. 595].

Surfaces that have undergone severe plastic deformation (as described in section 5.1.1) often exhibit highly work hardened sub-surface layers. During repeated sliding or rolling, surface or sub-surface initiated cracks may propagate along the deformed grain boundaries and eventually create spalled particles [29]. The remaining worn surface may be characterized by small pockets as shown in figure 18 from one of the hardbanding materials in Doerings experiments [30].

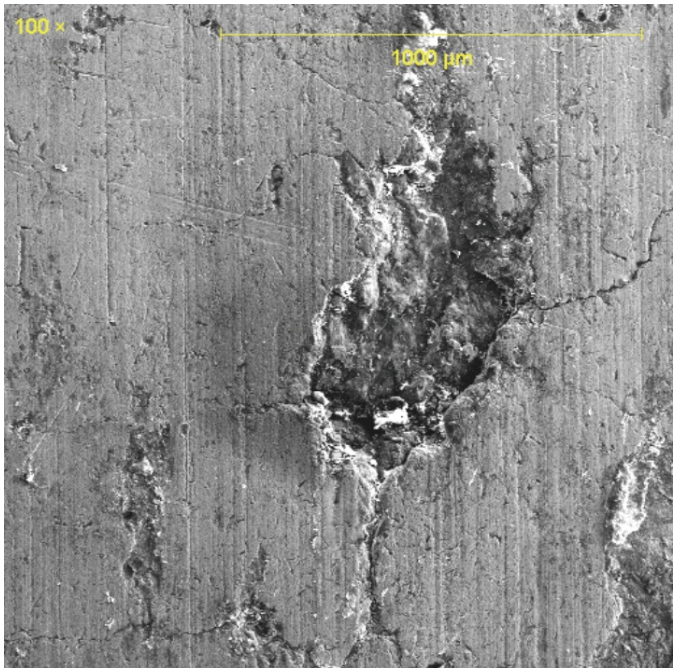

Figure 18: Spalled area on worn hardbanding surface tested in DEA-42 by Doering et al. [30].

5.2 Contact pressure

Contact pressure is one of the most important factors affecting casing wear and has been the topic for many research projects [35, 36, 37]. Even though casing wear can occur during several different drilling operations such as tripping and wire-line running, tool joint rotation is regarded as the main contributor to casing wear [35, 36].

When the first contact between tool joint and casing is made, the contact area is very small. In contrast to conformal contact, the initial area can be regarded as a line contact, which means very high contact pressure and wear rate. The width of the line contact increases as a wear groove is generated in the inner casing wall as shown in figure 19. The contact pressure and wear rate then stabilise at lower values [35, 36].

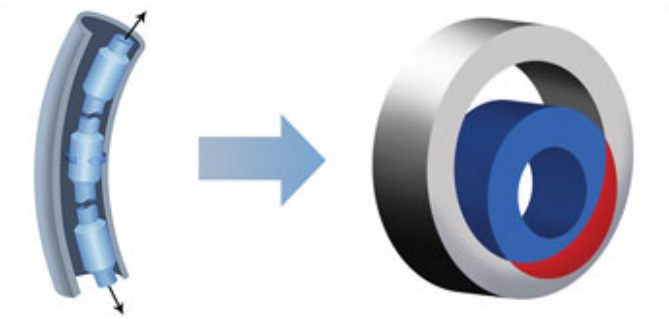

Figure 19: Tension of the drillstring increases the contact pressure on the inner casing wall and a wear groove is created [38].

The effect of contact pressures on casing wear rate was investigated by J. Steve Williamson [37] in 1981. His experiments showed good correlation between wear rate and contact pressure despite the data scattering in any wear test. For low contact pressures, abrasive wear was found to predominate. At high contact pressures, adhesive wear was identified as the primary mechanism. This shift in wear mechanism was observed at a contact pressure of approximately 1,4 MPa (200 psi), as shown in figure 20.

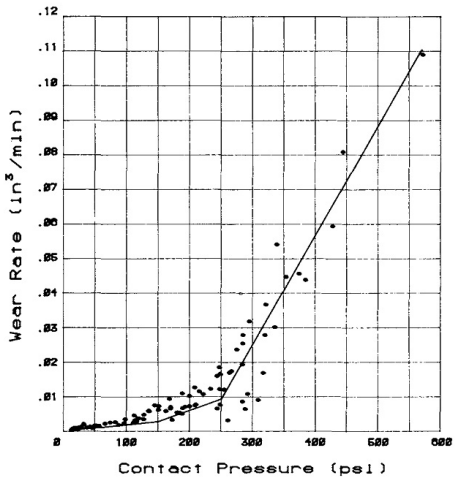

Figure 20: Casing wear rate as a function of contact pressure [37].

5.3 Drilling fluid

The single most important method of reducing friction and wear in a system is to add lubrication. In the case of drilling, the lubricant used is the drilling mud that acts as the intermediate medium between tool joint and casing. The lubricating properties are decided by several factors, including type of mud (oil or water based), weighting materials and additives.

Generally, lubrication reduce wear by creating a thin low shear strength layer of gas, liquid or solid between two moving surfaces. The lubricating effect is normally divided into three basic regimes:

Boundary lubrication - contact between surfaces even though a fluid is present.

Mixed lubrication - partial separation of the surfaces by a fluid film.

Hydrodynamic lubrication - surfaces are completely separated by a film created by a liquid phase, as for drilling mud, or a gaseous phase.

Stribeck curves, shown in figure 21, are used to evaluate which regime to expect in a system at given parameters, and consist of the coefficient of friction (vertical axis) as a function of fluid viscosity (Z), relative speed of surfaces (N) and contact pressure (P). The curve-region to the left is the boundary lubrication regime, characterised by high friction due to the absence of fluid film between the surfaces. This is often the case in high load, low speed contacts, -or if the viscosity of the fluid is low.
As the relative speed of the contacting surfaces increases (assuming constant load and fluid viscosity), a very thin lubricating film starts to partially separate the two surfaces. Roughness peaks and surface asperities are however still likely to cause

solid-solid contact. A sharp drop in coefficient of friction can usually be observed (figure 21).
Hydrodynamic lubrication is achieved when the speed is high enough to create a fluid film able to completely separate the surfaces. Transition to hydrodynamic lubrication regime is characterised by the lowest point on the curve, i.e where the friction reaches its minimum. The linear increase in coefficient of friction from this point and rightwards are determined by hydrostatic theory and fluid properties [29, 39].

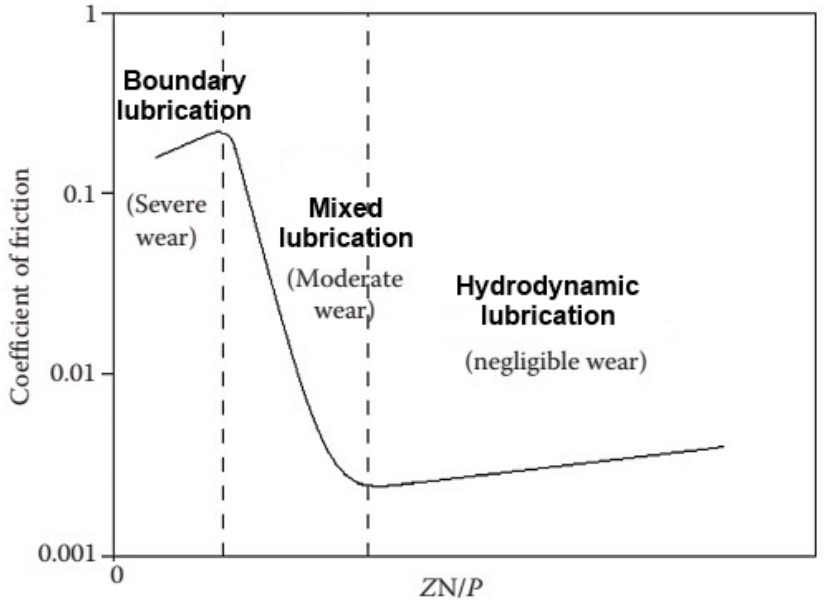

Figure 21: Stribeck curve with lubrication regimes and typical values of the friction coefficient. Redrawn from [39].

Drilling muds are divided into three main classes depending on the continuous phase that is used: gaseous, water-based and oil-based. While the former seldom is used in offshore drilling applications, the two latter are. The main difference between them is that water-based muds have a saline water-solution as a base, while the oil-based have a hydrocarbon base. Oil-based muds are in many situations preferred for their technical performance. Better lubrication properties, applicability in water-sensitive formations and high-pressure, high-temperature performance often outperforms the more environmental friendly water-based mud-class [40].

The properties of the drilling mud can be further controlled by the use of weighting material and additives. Weighting materials are used to control the mud density by adding soluble salts or finely ground mineral particles. Two of the most common ones are barite and ilmenite. Additives are used to control the mud viscosity, alkalinity, contaminant removal, lubrication and density in unweighted muds [40].

A study of the lubricating behaviour of a simple water-based drilling fluid in the contact between drill string and casing was recently done by B. J. Briscoe et al. [41]. By varying the contact loads, sliding velocities and mud compositions, two basic lubrication regimes were identified: At high contact loads (and low speeds), a regime characterised by the deposition of layers of solid clay onto the contacting surfaces was found. At low contact loads, the lubrication action was primarily provided by the base fluid. An intermediate region was found in between the two extremes, characterised by changes in fluid composition and rheology of the contact.

Optical investigations of the lubricating behaviour from the same experiments [41] revealed no traditional hydrodynamic or elastohydrodynamic fluid film formation. Instead, as the authors point out, the lubrication regimes can be classified as semi-fluid where the boundary components are important. This is further supported by the presence of "dry" clay particles on the worn surfaces, which indicate some sort of degeneration or phase separation of the mud when it moves through the contact.

Mud composition and its effect on casing wear was tested by G.M Bol [42] for Koninklijke/Shell E&P in a series of full-scale experiments in the late 80's. The following paragraphs summarize the most important results and conclusions from Bol:

Weighting materials in general decrease casing wear. Hard weighting particles in the series barite, iron oxide and quartz promote three-body abrasive wear, which wear rate is lower than two-body abrasive and adhesive wear. Within the three types of weighting particles, the quartz shows the highest wear due to its hardness, followed by iron oxide and barite (figure 22). It should also be noted that the small size of chalk and drilled solids reduce the film thickness between tool joint and casing, thus also the protection against adhesive wear.

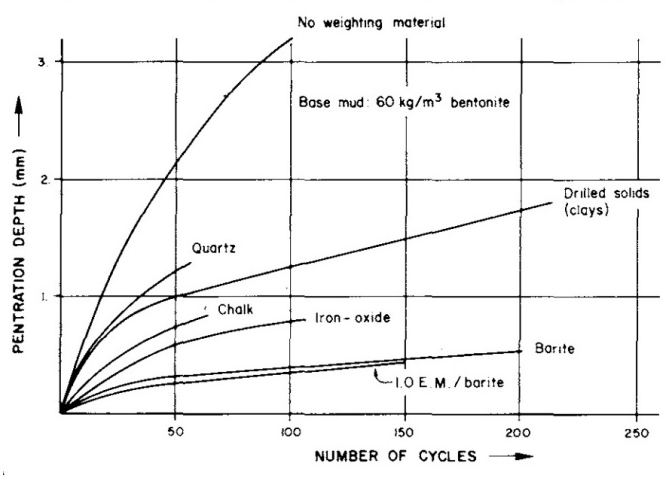

Figure 22: Effect of weighting materials on casing wear. Normal contact force of 8 kN [42].

Additives had no effect on the wear for weighted muds in Bol's experiments [42]. For unweigthed muds however, several effects were noted; all the commercially available lubricants tested showed the ability to prevent adhesive wear, thus also casing wear (figure 23). Additions of salt were also found to have a positive effect on casing wear. Bol indicated that the salts aid in the formation of a corroded layer and thereby partially prevented adhesive wear.

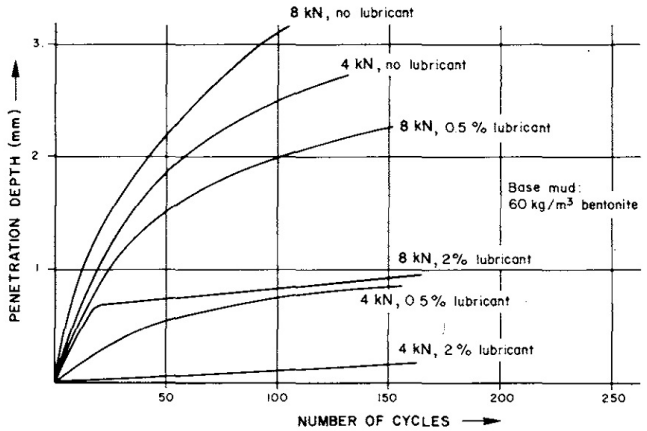

Figure 23: Effect of lubricant on casing wear (Bentonite suspension) [42].

Sand and silt in small quantities (2 to 4 vol%) has no or minimal effect on wear. It was concluded that in unweighted muds, the adhesive wear is so predominant that the abrasive effect of sand and silt is negligible. However, unweighted film-forming muds showed occasional peaks in the friction coefficient if the sand entered the contact zone. This had no effect on the overall wear rate. It should be noted that all of Bol's tests were performed with smooth, steel tool joints.

6 Wear models

In order to simulate casing wear the industry has developed casing wear simulation models that are meant to predict casing wear based on well design. Many of the simulation models used by the industry today are built upon empirical data collected from numerous of full-scale casing wear experiments, correlated with mathematical formulas. But for any other prediction model, the output is only as good as the input which means that the full-scale tests have to be accurate and replicate the field conditions as close as possible.

Even though there are slight differences in their simulation algorithms, many of the casing wear simulation models are mathematically deducted from the following sequence of equations:

Wear between surfaces of solids can be quantitatively described by the empirical approach proposed in the *Archard equation* [43] which states that the volume of removed material due to wear (WV) is proportional to the real contact area (A_r) times the sliding distance (SD):

$$WV = k \times SD \times A_r = k \times SD \times \frac{F_N}{H} \tag{1}$$

where the "k" coefficient, known as the "Archard coefficient", or "wear coefficient" is a proportionality constant which is used as an index of wear severity [29, p. 493]. The last term ($\frac{F_N}{H}$) includes total normal load (F_N) and the hardness of the softest contacting surface (H).

Most casing wear prediction models are basically assuming that the volume of removed metal from the inner casing wall is proportional to the frictional work done by the rotating tool joint, mathematically shown as [44]:

$$WV = \frac{\mu \times F_L \times \mathrm{SD}}{\epsilon} \tag{2}$$

where μ is the friction factor, F_L is lateral load per foot drill string and (ϵ) is the specific energy, defined as the energy required to remove one cubic inch of steel.

Hall et al. [45] simplified the model by introducing the "casing wear factor", which is defined as the ratio of friction factor (μ) to specific energy:

$$\mathrm{WF} = \frac{\mu}{\epsilon} \tag{3}$$

The sliding distance (SD) is defined as the total distance where there is contact between the tool-joint and the casing wall. This distance can be expressed as:

$$\text{SD} = \pi \times D_{tj} \times 60 \times RPM \times t \times f \tag{4}$$

where f is the fraction of time where the tool-joint touches a given element of the casing. D_{tj} is outside diameter of the tool joint, RPM is rotations per minute of the tool joint and t is rotating time.

The volume of removed material from the casing in time t hours is thus given by:

$$\text{WV} = WF \times F_L \times \pi \times D_{tj} \times RPM \times 60 \times t \times f \tag{5}$$

One of the most important empirical element in the casing wear simulation models is the "casing wear factor", which is a central parameter in the transition between theory and practice. Many oil companies and their software utilise large databases of wear factors. But as seen from the equations above, the wear factor is dependent of many other factors and may thus not necessarily fit a specific well design. In addition, with hardness (H) as the only material parameter, the influence of alloying elements and microstructure are disregarded since they do not necessarily modify the hardness, despite the fact that they can greatly influence the wear performance. Due to this uncertainty, wear factors are often given as a range, which may cause some unexpected results when applied in field [6].

Table 3: Overview of parameters used in wear prediction models. Units are given in "industry norm".

WV	=	Wear volume	$in.^3/ft$
WF	=	Casing wear factor	$in.^2/lbf$
F_L	=	Lateral load per foot	lbf/ft
D_{tj}	=	Tool joint outside diameter	$inch$
RPM	=	Rotary speed	$rotations\ per\ minute$
t	=	Rotating time	$hours$
f	=	Time fraction of TJ contact	

7 Experimental

7.1 Lab-scale hardbanding/casing wear tester

The aim of this master thesis was to create a lab-scale hardbanding and casing wear tester able to reproduce the wear mechanisms found in the full-scale experiments performed in the fall of 2012 [1]. A good lab-scale test design may provide an easier and faster way of testing existing and potential future hardbanding alloys.

Investigations of the worn full-scale samples from fall 2012 revealed that the rotation of the tool joint is the superior cause of wear on both hardbanding and casing (which is in accordance with previous observations by Bradley and Fontenot [35, 36]). Therefore, in contrast to the full-scale setup where both reciprocating and rotational movement of the tool joint were applied, the lab-scale tester should include rotational movement only.

A lab-scale a pin-on-ring (also known as block-on-ring) design was thus built using as base the original configuration of a Plint model TE-88 multi-station friction and wear tester, displayed in figure 24. The test configuration consist of a hardbanded pin specimen and a ring of casing. Whilst the ring specimen is mounted on a rotating shaft, the pin specimen is mounted stationary in 12 o'clock position with an applied normal load, schematically shown in figure 25.

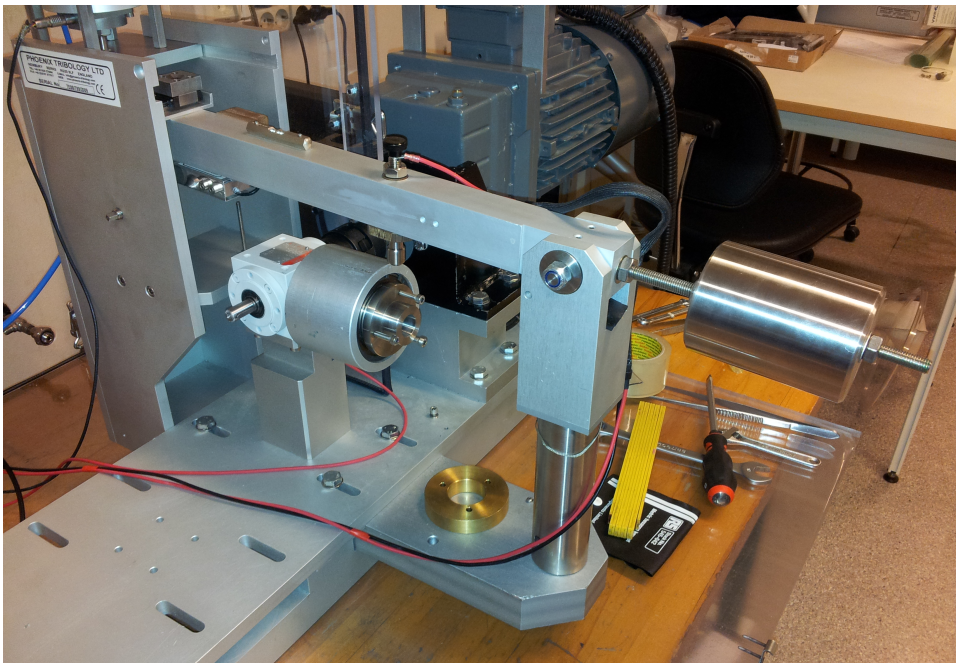

Figure 24: Overall view of the original TE-88 test machine in pin/block-on-ring mode.

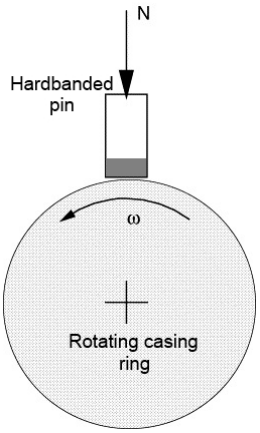

Figure 25: Pin-on-ring schematic overview. Redrawn from [46].

Since the original TE-88 setup does not provide any means for immersion of the ring specimen, a tube shaped container was built and attached to the test machine as shown in figure 26. The tube was made of PMMA (Poly(Methyl MethAcrylate)). This design ensured removal of wear debris from the pin/ring-contact zone, continuous lubrication of the ring surface and stirring of the mud-pool. As shown in figure 27, an hole in the upper tube wall made sure the pin could enter easily.

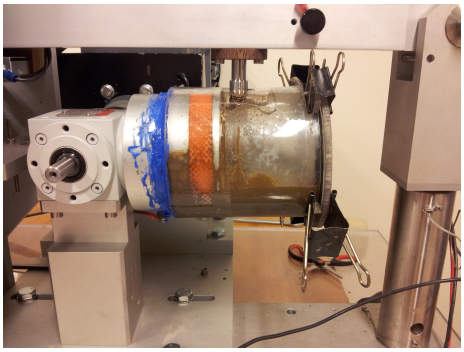

Figure 26: Test-tube attached to the original pin-on-ring configuration.

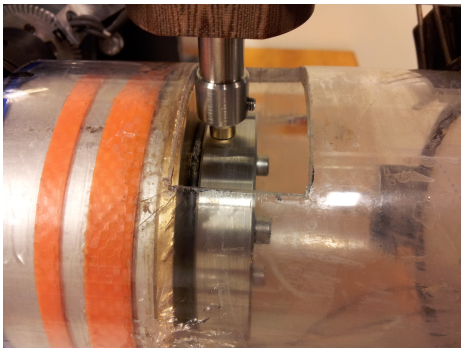

Figure 27: Pin placed on ring in tube setup.

7.2 Hardbanding pin

Five different hardbanding alloys of various brands and compositions were tested, in which all of them have previously been tested in the full-scale wear tester [1]. Pin specimens were cut out from hardbanded tool-joint samples provided by Trio Oiltec Services, as shown in figure 28. Cutting with pressurised water ensured minimal heat generation and thus preserved the as-welded microstructure. After cutting, the hardbanded end of the pins were machined to create a tip radius, shown in figure 29. The tip radius provides a method of controlling contact geometry, thus also contact pressure since the normal load limits of the TE-88 is restricted to a maximum of 1000 N. The radius for each test program is given in section 7.6.

Figure 28: Pin samples cut out from a tool joint section.

Figure 29: Hardbanded pin with machined tip radius.

Chemical composition and hardness of the five hardbanding materials tested are given in table 4 below.

Table 4: Composition, main particles and hardness of the five hardbanding materials.

Sample name	**Hardbanding composition (matrix and particles combined)**	**Type of particles**	**Hardness [HV-02]**
HB A	Steel (6% Ti, 5%Cr, 1.5%C, 1.5%Mo, 1%Mn)	Ti-cermet	690
HB B	Steel (5%Nb, 4%B, 2%Ni, 1%C)	NbB	840
HB C	Steel (2%Nb, 1.4%Ni, 1.3%C, 1%B, 0.3%Si)	NbB	690
HB D	Steel (7%Cr, 6%Ti, 2%C, 1%Mn, 1%Mo, 0.3%V)	Ti-cermet	650
HB E	Steel (5.5%Nb, 5.5%Cr, 1.3%C, 1%Si, 1%Mn, 0.5%V)	Nb-cermet	730

7.3 Casing ring

Ring specimens, representing a casing tube, were made from a quenched and tempered AISI 4130 medium carbon steel rod (tempered martensite microstructure similar to P-110 casing grade). Its chemical composition and mechanical properties are given in table 5 and 6 respectively. Outer diameter of the rings was 80 mm, while the inner diameter for TE-88 shaft mounting was 36 mm. Additionally, three holes for fixing the ring to the shaft were made. Figure 30 shows a finished ring ready for testing.

Table 5: Chemical composition of AISI 4130. All numbers in wt%.

C	Mn	Si	P	Si	Cr	Ni	Mo	V	Cu	Al
0.3	0.57	0.28	0.011	0.006	1.08	0.15	0.237	0.004	0.14	0.026

Table 6: Mechanical and surface properties of the ring specimens.

Hardness at surface		244	HV
Yield strength		572	MPa
Tensile strength		738	MPa
Elongation		24.2	%
Surface roughness	Ra	0.4807	μm
	Rz	2.8920	μm

Figure 30: Front and side view of a machined ring specimen.

7.4 Contact geometry and pressure

The properties of the pin/ring interaction were calculated according to Hertzian contact theory, the following assumptions are thus made [29]:

- Material strains are small and within the elastic limit.
- Contact area are much smaller than the characteristic radius of the body.
- Non-conforming surfaces [1].
- Surfaces are frictionless.

Figure 31 provides an overview of the already mentioned pin and ring dimensions. The spherical pin end and the cylindrical ring results in an elliptical contact which dimensions and contact pressures can be calculated as follows [29]:

Elliptic contact area dimensions are given by the two radii a and b, expressed as:

$$a = k_1 \left(\frac{3WR'}{E'} \right)^{1/3} \tag{6}$$

$$b = k_2 \left(\frac{3WR'}{E'} \right)^{1/3} \tag{7}$$

where R' and E' are the reduced radius of curvature and E-modulus respectively. W is the normal load, and k_1 and k_2 are contact coefficients.

Maximum and mean Hertzian contact pressures can now be calculated:

$$p_{max} = \frac{3W}{2\pi ab} \tag{8}$$

$$p_{mean} = \frac{W}{\pi ab} \tag{9}$$

It should be mentioned that the maximum contact pressure (p_{max}) is at the initial contact. As wear evolves this pressure will decrease.

Complete Hertzian equations are given in appendix B.

[1] A non-conforming contact is one that involves two bodies of such dissimilar shape that, under zero load, they only touch at one point (or a line).

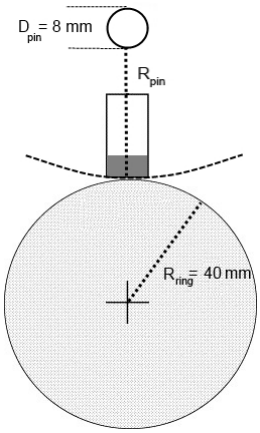

Figure 31: Pin and ring sample geometry.

7.5 Slurry

All experiments were performed with a slurry consisting of an oil-based drilling mud and sand mixed together. The mud used was provided by Mi-Swaco (Schlumberger) and is a Versatec oil-based mud with specific gravity (SG) of 1.57 and a Oil-Water-Ratio (OWR) of approximately 80/20. Its complete composition are given in table 7, and table 8 shows the rheology profile for this kind of mud system. The sand was SiO_2 of 36 grit, i.e an average particle diameter of 500 μm.

Each experiment was run with a separately mixed slurry batch that included approximately 200 ml of mud mixed together with sand, which amount is given in the individual test-program descriptions that follows in section 7.6.

Please note that an attempt to add the sand and mud separately to the testing tube was made for the first test run, i.e Hardbanding A/Casing A. This was unsuccessful as the sand did not mix with the mud, and turned out to be present as a big sand ball at the bottom of the tube.

Table 7: Composition and properties of Versatec drilling mud.

Type	Versatec 1.57 SG	
Main constituents		
Petroleum destilate	80	%
Freshwater	20	%
Calcium Chloride	1-5	%
Calcium Hydroxide	1-5	%
Miscellaneous additives	1-5	%
Density	1.3	g/cm^3

Table 8: Rheology of a typical oil-based drilling mud (temperature = 50 °C). Provided by Mi-Swaco [47].

600 rpm	0.050	kg/cm^2
300 rpm	0.030	kg/cm^2
200 rpm	0.023	kg/cm^2
100 rpm	0.015	kg/cm^2
6 rpm	0.0048	kg/cm^2
3 rpm	0.0039	kg/cm^2
10 seconds gel	0.0073	kg/cm^2
10 min gel	0.0190	kg/cm^2
Plastic viscosity	40	cP
Yield point	0.011	kg/cm^2

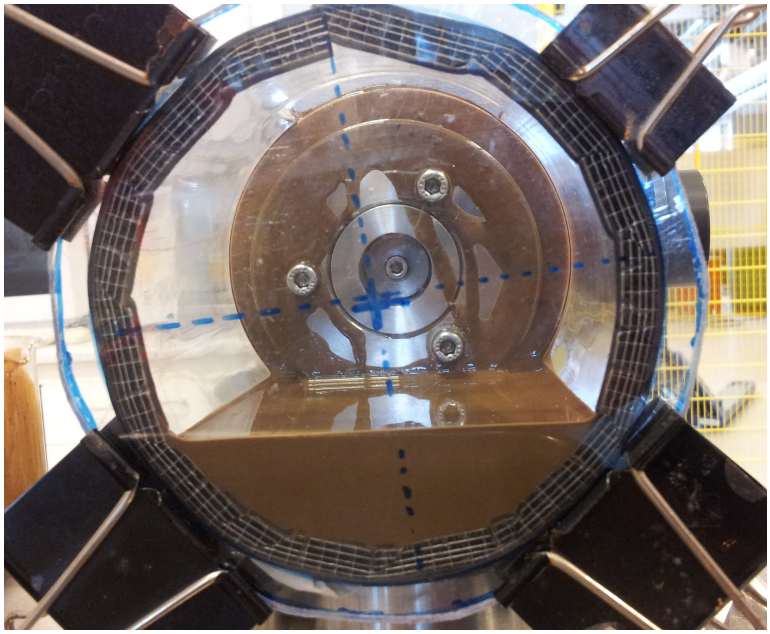

Figure 32: Testing tube in TE-88 with mounted ring sample and slurry before starting the test.

7.6 Test program

Three different test programs were used in the attempt to reproduce the wear mechanisms that are known to be present in the hardbanding/casing/mud-complex system as described in section 5.1. Unfortunately, due to the limited availability of hardbanding pin specimens, it was carried out only one parallel for each test program. Ideally, a second or even a third parallel should have been carried out to ensure test repeatability. However, since each program includes five different hardbanding materials, comparison of their wear behaviour may increase the test validity.

7.6.1 Program 1

The parameters for the initial test program were mainly based on small-scale experiments conducted by Doering et al. [30] in 2011 that showed the ability to reproduce in-field and full-scale wear mechanisms. Program 1 was thus mainly designed to create the same mean and maximum contact pressure as in Doerings experiments, which was 390 Mpa and 590 MPa respectively. The amount of sand was set to 17 wt%, and a duration of 30 min was set to obtain a total sliding distance of 2262 m, also based on Doering.

Table 9: Test parameters for program 1.

Pin tip radius	400	mm
Normal load at pin	750	N
Contact pressure mean	390	MPa
Contact pressure max	590	MPa
Duration	30	minutes
RPM ring	300	
Sliding speed	126	cm/s
Sliding distance	2262	m
Mud	Versatec	
Abrasive	17 wt% SiO_2	

7.6.2 Program 2

Test program 2 was based on observed wear tracks on the samples from program 1 (see section 8.2). Due to the absence of adhesive wear on the ring (casing) specimens and no indications of spalling on the worn pin surface, it was decided to increase the normal load on the pin from 750 N to 950 N. According to Hertzian theory this should increase mean and maximum contact pressure to 430 MPa and 640 MPa respectively. Moreover, the amount of sand was reduced to 6 wt% in order to promote more severe plastic deformation, thus (possible) also fatigue (spalling) wear.

Due to extensive generation of heat from frictional forces in program 1 and sufficient pin weight loss (to use it as a metric), the test duration was reduced to 15 minutes with a resulting sliding distance of 1131 m.

Table 10: Test parameters for program 2.

Pin tip radius	400	mm
Normal load at pin	950	N
Contact pressure mean	430	MPa
Contact pressure max	640	MPa
Duration	15	minutes
RPM ring	300	
Sliding speed	126	cm/s
Sliding distance	1131	m
Mud	Versatec	
Abrasive	6 wt% SiO_2	

7.6.3 Program 3

Program 3 parameters were based on the observed wear pattern on samples from program 2, which (still) lacked the wanted degree of adhesive and fatigue wear. The most important difference is the increased mean contact pressure from 430 MPa to 520 MPa. Due to the load limit of the TE-88 machine, this had to be obtained by a reduction of pin-end radius from 400 mm to 200 mm. The ring specimens remained the same as for program 1 and 2. Moreover, based on information from Statoil, it was decided to use 12 wt% sand in the slurry. Test duration of 15 minutes remained unchanged, thus also sliding distance.

Table 11: Test parameters for program 3.

Pin tip radius	200	mm
Normal load at pin	950	N
Contact pressure mean	520	MPa
Contact pressure max	780	MPa
Duration	15	minutes
RPM ring	300	
Sliding speed	126	cm/s
Sliding distance	1131	m
Mud	Versatec	
Abrasive	12 wt% SiO_2	

7.7 Sample extraction and preparation

Sample pieces from all ring and pin specimens were prepared for both surface and cross section examination. The worn surfaces were cleaned properly with acetone and ultrasonic bath before scanning electron microscope (SEM) investigations. For cross section investigations both ring and pin samples were hot mounted with edge-retaining Struers Polyfast mounting resin. Grinding was done with SiC-papers of grades P80, P120, P240, P500, P800, P1000, P2400 and polished with 3 and 1 μm diamond polishing spray suspension. The microstructure was made visible by etching with 2% nital ($2\%HNO_3 + ethanol$).

Hardness measurements were taken with a Mitutoyo HM-210/220 (Micro Vickers hardness testing machine). Bulk measurements were done with 2 kg force, while the measurements in the deformed sub-surface layers were done with 0.05 kg force.

8 Results

This section consist of two parts: The first part presents the main results from the full-scale experiments carried out in the fall of 2012 [1]. These results serve as reference wear patterns. The second part presents the results from the three different lab-scale test programs described in section 7.

The images presented in the main text are chosen as they are representative for all the samples from the respective test programs. Additional images from all samples can be found in appendix C. The sliding direction is indicated by arrows where necessary in the images.

The rest of this page is intentionally left blank for improved readability of the upcoming sections.

8.1 Full-scale wear test results: reference samples

The full-scale tests were done with a normal load of 330 kg, tool joint rotational speed of 140 rpm and test duration of 8 hours. The drilling mud was Versatec oil-based. Sand was present in the system to some extent [1].

Figure 33 shows the most common wear patterns found on the hardbanding surfaces and cross sections from the full-scale tests [1]. As figure 33a and 33b show, the wear surface consists of a mix between flowed material by adhesion and cracks oriented perpendicular to the direction of sliding. Some shallow pits can also be observed. Limited amount of abrasive wear marks are visible on some areas. Cross section analysis (figure 33c and 33d) reveal regularly spaced cracks that extend down to undisturbed bulk microstructure. Larger spalled particles are found in the work-hardened surface layer.

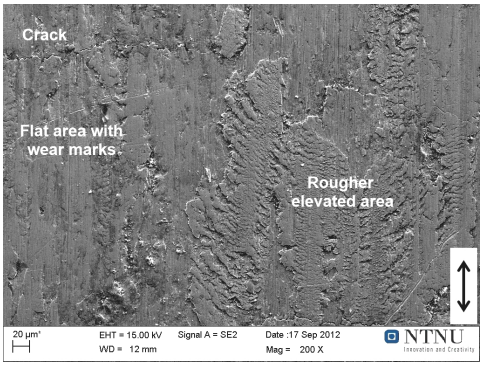

(a) Hardbanding surface, 200X.

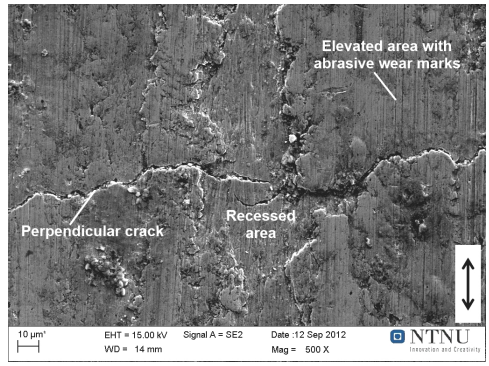

(b) Hardbanding surface, 500X.

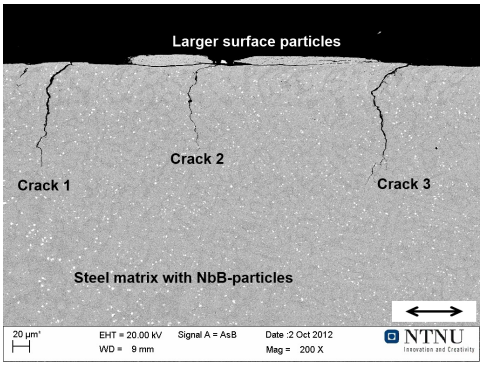

(c) Hardbanding cross section, 200X.

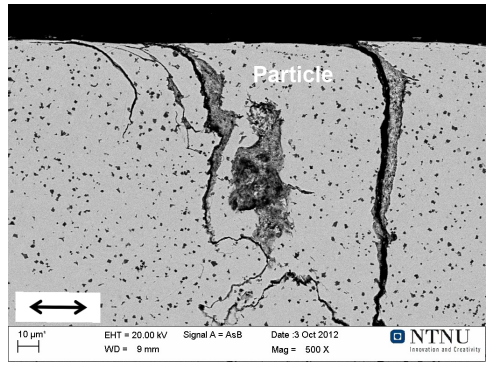

(d) Hardbanding cross section, 500X.

Figure 33: SEM images of some worn hardbanding samples from full-scale tests.

The most common wear patterns from the worn full-scale casing samples are displayed in figure 34 below. Pit formations and distinct plastic flow of material by adhesive wear are clearly present, and possibly also some degree of fatigue wear. In addition, some flatter areas with smoother linear abrasive wear marks can be seen.
Cross section images (figure 34c and 34d) reveal a significant plastically deformed layer. Three different zones can be distinguished, a heavily deformed zone that includes particles from the hardbanding, a deformed zone with a really fine grained microstructure and a partially deformed zone. The depth of material displacement is in the range 50-70 μm.

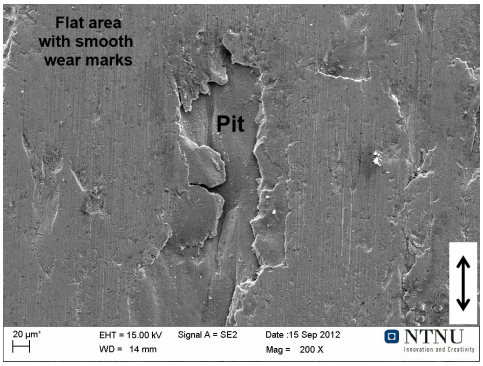

(a) Casing surface, 200X.

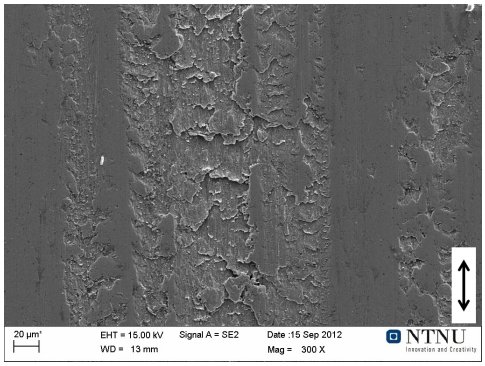

(b) Casing surface, 300X.

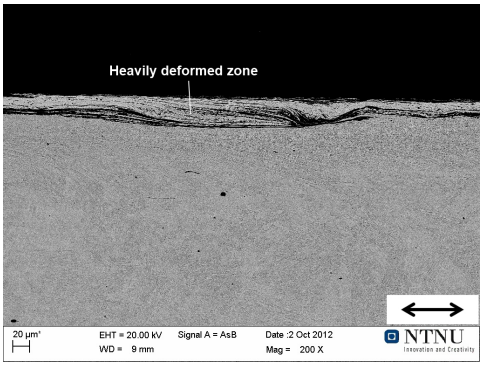

(c) Casing cross section, 200X.

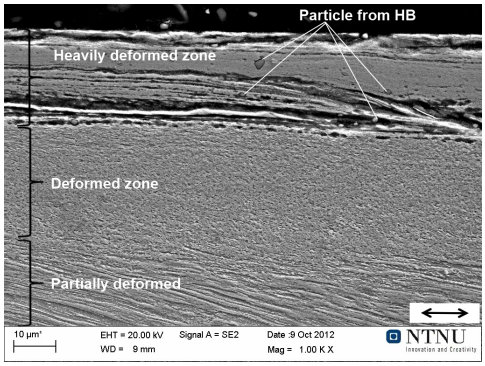

(d) Casing cross section, 1000X.

Figure 34: SEM images of some worn casing samples from full-scale tests.

8.2 Test program 1

Data from test program 1 are presented in table 12. Load at pin, friction at pin and CoF are averaged values. Figure 35 shows averaged CoF and pin weight loss graphically.

Table 12: Data from test program 1.

	Test A	**Test B**	**Test C**	**Test D**	**Test E**	
Weight change						
Pin	-0.0017	-0.0014	-0.0023	-0.0021	-0.0013	[g]
Ring	-0.1	-0.2	-0.1	-0.1	-0.1	[g]
Sand content	17	17	17	17	17	[wt%]
Load at pin	744	744	741	741	748	[N]
Friction at pin	67	72	73	88	65	
CoF	0.0902	0.0962	0.0988	0.1186	0.0869	

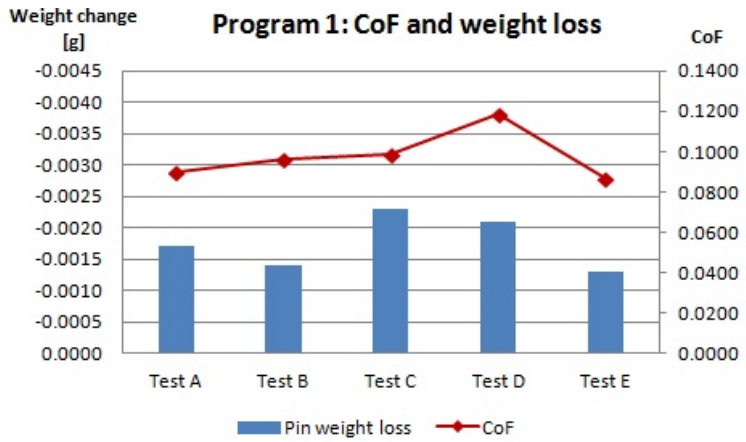

Figure 35: Test program 1: CoF and pin weight loss.

8.2.1 Worn samples

Figure 36 below shows some worn hardbanding surfaces from test program 1. All the hardbanding samples show more or less the same type of wear. The hardbanding wear surfaces consist mainly of mild adhesive damage that includes dragged particles as showed in figure 36a. More roughened areas can be found at the edges of the contact zone (see figure 66 in appendix C). Hardbanding cross section images mainly show an undisturbed microstructure, but as figure 36b reveals, some of the hardbanding particles have been uncovered by the wear process.

The casing samples (figure 37) consist of linear abrasive wear patterns that cover most of the surfaces. However, some areas also include plastically flowed material by adhesion. The latter is visible as mild microstructural displacement in figure 37b.

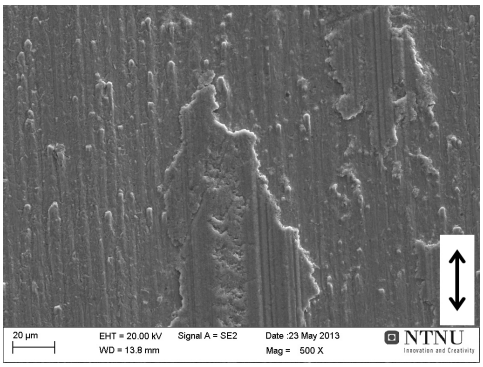

(a) Hardbanding surface, 500X.

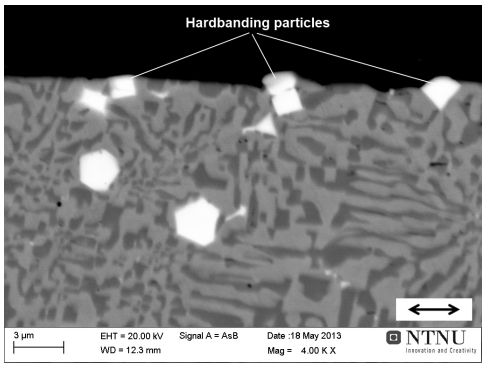

(b) Hardbanding cross section, 4000X.

Figure 36: SEM images of some worn hardbanding samples from program 1.

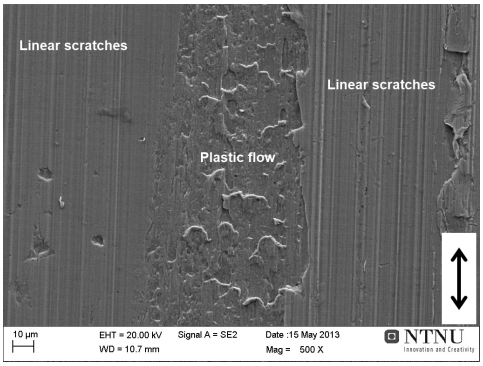

(a) Casing surface, 500X.

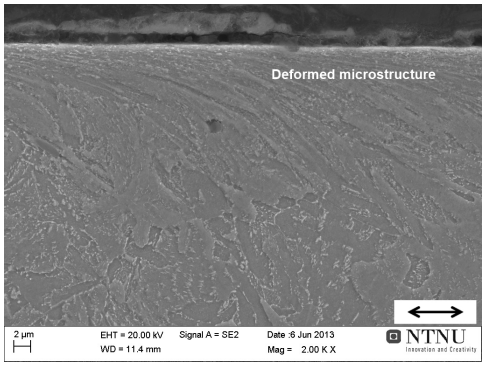

(b) Casing cross section, 2000X.

Figure 37: SEM images of some worn casing samples from program 1.

Micro hardness measurements taken 20 μm below the worn casing surface are shown in table 13 below.

Table 13: Hardness of worn casing samples from program 1, 20 μm below worn surface. Bulk hardness of 244 HV.

	Casing A	Casing B	Casing C	Casing D	Casing E
20 μm below surface	353	261	267	266	248

8.3 Test program 2

Recorded parameters from test program 2 are presented in table 14. Pin weight loss and CoF are graphically presented in figure 38. It should be reminded that the test duration was reduced from 30 minutes (program 1) to 15 minutes in program 2.

Table 14: Data from test program 2.

	Test A	**Test B**	**Test C**	**Test D**	**Test E**	
Weight change						
Pin	-0.0023	-0.0023	-0.0042	-0.0029	-0.0024	[g]
Ring	0.0	0.0	0.0	-0.1	0.0	[g]
Sand content	6	6	6	6	6	[wt%]
Load at pin	950	957	942	950	954	[N]
Friction at pin	90	111	106	78	112	
CoF	0.0952	0.1156	0.1125	0.0819	0.1170	

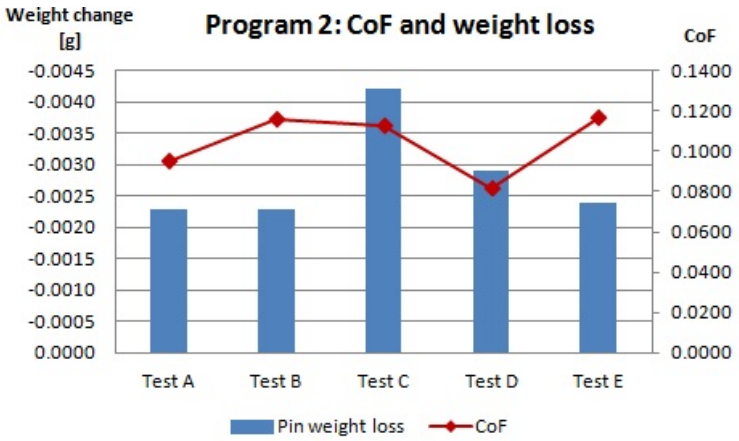

Figure 38: Test program 2: CoF and pin weight loss.

8.3.1 Worn samples

Figure 39 displays the worn hardbanding samples from test program 2. The worn hardbanding samples show both traces of abrasive wear by the presence of linear scratches, and areas of smeared material by adhesion. The surface of hardbanding B also includes a larger spalled area located in the center of the pin (figure 39a). Cross section images reveal some cracking and spalling in the worn hardbanding surface, as shown in figure 39b.

The worn casing samples (figure 40) consist of significant plastic flow and ridge formations visible on the surface, while a clearly deformed surface layer can be found in cross section view. Particles from the hardbanding counterpart has been found in this layer (EDS analysis provided in appendix D).

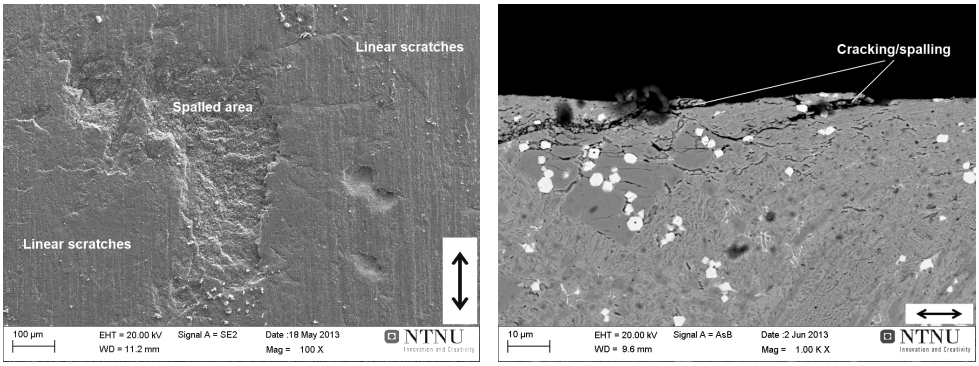

(a) Hardbanding surface, 100X. (b) Hardbanding cross section, 1000X.

Figure 39: SEM images of some worn hardbanding samples from program 2.

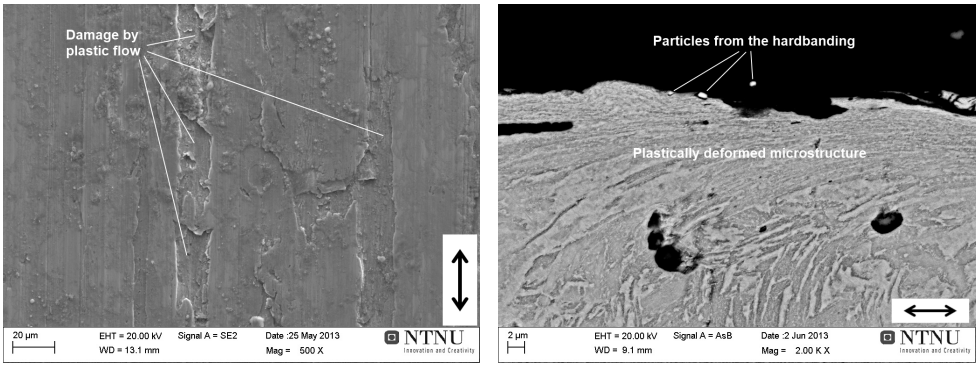

(a) Casing surface, 500X. (b) Casing cross section, 2000X.

Figure 40: SEM images of some worn casing samples from program 2.

Micro hardness measurements taken 20 μm below the worn casing surface are shown in table 15 below.

Table 15: Hardness of worn casing samples from program 2, taken 20 μm below worn surface. Bulk hardness of 244 HV.

	Casing A	Casing B	Casing C	Casing D	Casing E
20 μm below surface	264	356	384	337	291

8.4 Test program 3

Test data from program 3 are presented in table 16. Pin weight loss and CoF are displayed in figure 41.

Table 16: Data from test program 3.

	Test A	**Test B**	**Test C**	**Test D**	**Test E**	
Weight change						
Pin	-0.0012	-0.0012	-0.0038	-0.0042	-0.0016	[g]
Ring	-0.1	-0.1	-0.2	-0.1	-0.2	[g]
Sand content	12	12	12	12	12	[wt%]
Load at pin	951	952	948	938	937	[N]
Friction at pin	87	87	94	114	80	
CoF	0.0912	0.0916	0.0995	0.1216	0.0859	

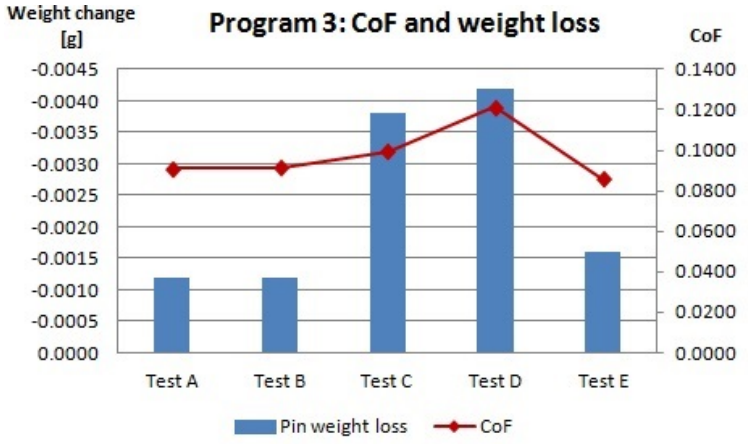

Figure 41: Test program 3: CoF and pin weight loss.

8.4.1 Worn samples

The worn hardbanding samples from test program 3 include many of the same wear patterns as the hardbanding samples from program 2, but at the same time the different mechanisms are more easily distinguished. As figure 42a shows, the hardbanding surfaces have traces of adhesive wear (plastically deformed areas) and minor abrasive scratches parallel to the direction of motion. Adhesive wear is also confirmed by the work-hardened layer visible in figure 42b. Similar to hardbanding B in program 2 (figure 39a) the wear surface of hardbanding B also included a larger spalled area loacted in the center of the pin.

The casing samples show plastic flow, ridge formations and some linear abrasive scratches (figure 40a). Cross section images reveal plastically deformed (work-hardened) surface layers that (occasionally) include particles from the hardbanding counterpart (figure 43b).

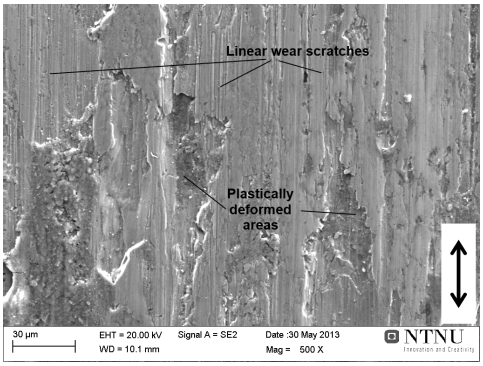

(a) Hardbanding surface, 500X.

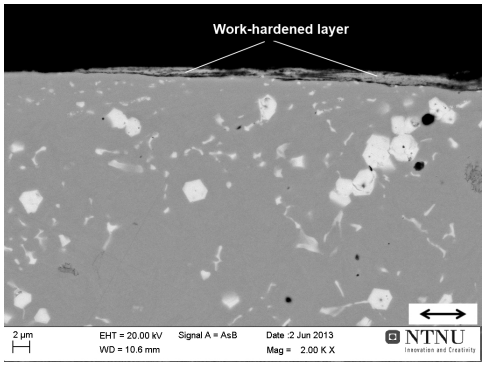

(b) Hardbanding cross section, 2000X.

Figure 42: SEM images of some worn hardbanding samples from program 3.

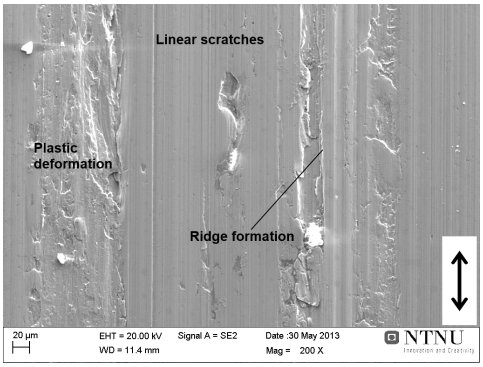

(a) Casing surface, 200X.

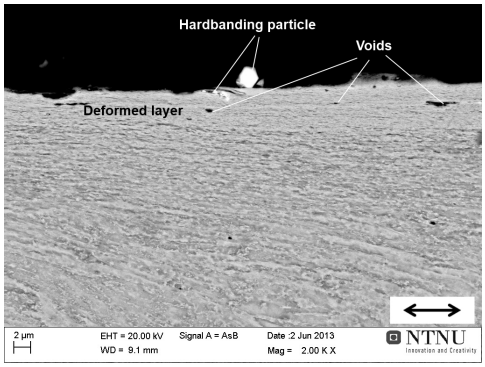

(b) Casing cross section, 2000X.

Figure 43: SEM images of some worn casing samples from program 3.

Micro hardness measurements taken 20 μm below the worn casing surface are shown in table 17 below.

Table 17: Hardness of worn casing samples from program 3, 20 μm below worn surface. Bulk hardness of 244 HV.

	Casing A	Casing B	Casing C	Casing D	Casing E
20 μm below surface	293	323	390	302	336

9 Discussion

9.1 Wear characterisation

The most important step in the process of reproducing wear mechanisms is to understand the wear mechanisms of interest. In this thesis, the full-scale samples presented in section 8.1 serve as reference samples. Test program 1, 2 and 3 were all designed to produce the same wear mechanisms as seen in full-scale. The following sections will characterise and summarise the wear mechanisms that are present in the different test programs.

9.1.1 Full-scale tests

The wear surfaces of the five hardbanding materials from the full-scale tests all showed more or less the same kind of wear behaviour. Adhesion and abrasion were the primary mechanisms, whereas the former resulted in the development of a work-hardened surface-layer, which later caused checking and spalling. The checking or cracking often covered the whole hardbanding surface, and was oriented perpendicular to the wear direction as shown in figure 33b. These cracks were also found to be the prominent feature in cross section examinations (figure 33c and 33d).

The casing samples on the other hand, with its lower hardness and higher ductility showed far more plastic flow and ridge formation than the hardbanding counterparts, making adhesive wear the predominant mechanism. Some abrasive patterns in the form of linear scratches could also be found (figure 34a), however in a more subtle manner. The severe plastic deformation was also confirmed by cross section analysis (figure 34d). Work-hardened layers in the range of 50-100 μm in thickness were found in all of the casing samples. The upper 50 μm often consisted of a mixture of deformed casing microstructure, voids and particles from the hardbanding counterparts, which are typical for severe adhesive wear, or galling.

9.1.2 Test program 1

As shown in figure 36a the worn hardbanding (pin) samples features two types of wear pattern. The sections of smeared material indicate that flow of material and thus adhesive wear has been present. Secondly, particles seem to have been dragged along the surface parallel to the sliding direction.
The adhesive wear is in accordance with the full-scale samples, however it appears to have occurred to a lesser extent. The dragged particles on the other hand have not been seen on any of the full-scale hardbanding samples. High magnification cross section images as figure 36b and their size of approximately 2 μm prove that they originate from the hardbanding material itself (thus not from the slurry).

The casing surfaces from the same test program showed a combination of adhesive and abrasive wear (figure 37a). Similar to the full-scale casing samples, the adhesive mechanism is the most prominent of the wear types. However, its severity is much lesser than seen in full-scale. Cross section analysis as in figure 37b reveal

only a mild degree of plastically deformed microstructure, which depth is approximately 2-6 μm. No mixed zone of voids and hardbanding particles could be found on any of the casing samples.

9.1.3 Test program 2

Similar to program 1, the worn hardbanding surfaces from program 2 showed adhesive and abrasive wear patterns. Its severity does however seem to be somewhat larger in the form of sharper edges and more distinct wear patterns on the surface. Dragged particles are present on some of the hardbanding material surfaces.
One of the hardbanding samples (HB-B) also had an area of spalled material in the pin center, as shown in figure 39a. It was expected that if spalling was to happen, it would be hardbanding B due to its brittle nature. Cross section image (figure 39b) of the same hardbanding revealed occasional small cracks in the surface layer. Whether they were caused by the wear process or simply an original feature is difficult to say.

On the casing samples a mix of adhesive and abrasive wear was found. However, as figure 40a shows, more prominent ridge formations and deeper reaching plastic flow of material seem to have occurred (compared to program 1). This is also seen by cross section analysis (figure 40b) where the surface microstructure is clearly displaced to a depth of 6-12 μm. Some voids and occasional particles from the hardbanding counterpart could be observed in the upper layer, indicating galling wear.

9.1.4 Test program 3

Hardbanding samples from this test program still show the characteristics of adhesive and abrasive wear (figure 42a). Plastic flow of material on the hardbanding surfaces seem to include a larger number of shallow pits that may be the result of work-hardening. A spalled area could be found in the center of hardbanding B, as seen in test program 2, and some areas of dragged particles can still be found on some of the samples. Cross section analysis (as in figure 42b) reveal that a work-hardened layer has been formed on many of the samples.

The casing surfaces primarily show significant plastic flow, typical of galling wear (figure 43a). Some linear scratches by abrasion are visible, but with damage notably lesser than the damage caused by adhesion (galling). Some areas of the casing surface appear smoothed. Cross section examination (figure 43b) clearly shows a work-hardened layer reaching 10-22 μm into the bulk microstructure. The upper part includes voids and particles from the hardbanding. Bending of the original martensitic microstructure in the direction of sliding (right to left in the figure) is evident.

9.2 Comparison of the test programs

A comparison of the wear characteristics of the different test programs is shown in table 18 below. Adhesive wear was one of the most important mechanisms to reproduce due to its major influence in the full-scale sample surfaces. Program 1, with the lowest contact pressure was not able to produce any significant adhesion on either the hardbanding or casing surfaces (2-6 μm work-hardened layer). Program 2, with its lower sand content and increased contact pressure definitely created more adhesive damage on the sample surfaces and especially the casings, which work-hardened significantly more than in program 1 (see figure 44). The depth of displacement in program 2 casings was in the range 6-12 μm. Program 3 maintained the degree of work-hardening of the casing samples seen in program 2 (14-22 μm displacement depth in some samples), but also created a work-hardened layer on the hardbanding materials. This may be explained by the increased contact pressure in program 3. Another common feature for the casing samples from program 2 and 3 is the presence of hardbanding particles and voids in the work-hardened layers, which is typical for galling wear.

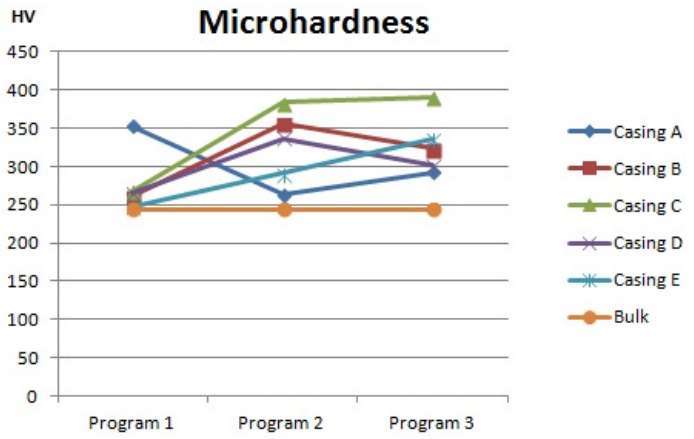

Figure 44: Microhardness measurements taken 20 μm into the work-hardened layers. Load was 0.05 kg. All values in Vickers.
Remember that Test A in program 1 was run basically without sand due to improper mixing of the slurry as mentioned in section 7.5.

Abrasive wear is present in all the samples, both full-scale and lab-scale. Program 1 (highest sand content) has the most apparent abrasive wear marks, but it can be questioned whether or not this is due to the abrasion itself or simply the lack of adhesive wear.

Cracking and spalling of the hardbanding surfaces were one of the most prominent features in the full-scale experiments. As described in section 5.1.3, spalling occurs when cracks initiate at defects in the microstructure, are allowed to propa-

gate and eventually creates particles that can escape. In the lab-scale experiments, test program 2 and 3 were able to create spalling in one of the hardbanding materials, namely HB-B, which is the most brittle due to its Boron content. The spalled areas were located close to the center of the pin and can thus be assumed to have experienced the highest contact pressures and longest contact duration. It is reasonable to believe that a longer overall test duration would have resulted in more fatigue wear (spalling and cracking) in the hardbanding samples, and a potential future test program should include longer testing times.

Table 18: Comparison summary of the wear characteristics.

	Full-scale		**Program 1**		**Program 2**		**Program 3**	
Surface characteristic	**HB**	**Casing**	**HB**	**Casing**	**HB**	**Casing**	**HB**	**Casing**
Adhesive wear	Severe	Severe	Little	Little	Moderate	Moderate	Severe	Severe
Abrasive wear	Minimal	Little	Yes	Yes	Minimal	Little	Little	Minimal
Cracking/spalling	Yes	No	No	No	On HB-B	No	On HB-B	No
Work-hardened layer	Yes	Yes	No	Minimal	Minimal	Yes	Yes	Yes

9.3 Contact pressure

Three different initial contact pressures were used in these experiments; 390 MPa, 430 MPa and 520 MPa. From the wear characterisation above it can be seen a shift from an more abrasive wear regime in program 1, to an adhesive wear regime in program 2 and 3. This is in accordance with the experiments by Williamson [37] where high contact pressures promoted adhesive wear, while low contact pressures promoted abrasive wear. It should be mentioned that Williamson observed this shift at 1.4 MPa contact pressure, which is surprisingly low. Williamson did not include how the calculations of the contact pressure were done.

Another interesting observation is the presence of the dragged particles on the hardbanding samples. Program 1 hardbanding surfaces included large sections of this tear-drop pattern (see figure 67 in appendix C). The same pattern was also found in samples from program 2 and 3, but to much lesser extent. It may be that lower contact pressures are only able to move the particles along the surface, parallel to the sliding direction, while higher contact pressure push them further into the hardbanding body, or more likely: pulling them out. The latter may explain the presence of hardbanding particles in the worn casing samples.

9.4 Sand content

Since test program 1, 2 and 3 primarily were designed to reproduce the full-scale wear mechanisms, the sand content was chosen thereafter and unfortunately left any systematic approach behind. Still, some observations can be made. Program 1 (17 wt% sand / 9 vol%) caused the largest degree of abrasion on the surfaces, but it can be questioned whether or not it is on the expense of adhesion, or due to lack of adhesion (too low contact pressure). Program 2 had the lowest amount of sand (6 wt% / 3 vol%), and as expected, showed little to minimal abrasive damage on

the samples. The sand content was increased in program 3 (12 wt% / 7 vol%), but no significant change in abrasive damage (compared to program 2) could be found.

From Bol's experiments [42] (see section 5.3) it was concluded that small quantities (2-4 vol%) of sand and slit had no or minimal effect on wear due to adhesive wear predominance. This can also be said to be the trend for the three test programs performed in this thesis. It is reason to believe that an increase in contact pressure prevents the sand particles to enter the contact, especially if the contact area is small, e.g a pin.
Regarding the full-scale reference experiments, the full-scale sample geometry may have allowed for sand to be trapped in-between the rotating tool joint and the casing. The sand particles may thus have entered the contact even at high contact pressures with increased amount of cutting and ploughing as a likely result. Nevertheless, uncertainties with respect to sand content in the full-scale experiments in addition to the differences in test setup and contact geometry (between full-scale and lab-scale) makes it difficult to draw any conclusions on this topic.

9.5 Test duration

The test duration of 30 minutes for program 1 and 15 minutes for program 2 and 3 was sufficient to use pin-weight loss as a metric. However, as briefly mentioned already, work-hardening with subsequent cracking and spalling require both sufficient load and a certain number of load cycles (section 5.1.3). It is reasonable to assume that longer test duration would have created more fatigue wear in the form of spalled particles on the hardbanding surfaces and more distinct work-hardened layers in the casing samples. The latter would also include a larger number of hardbanding particles, as seen in the full-scale samples, since more particles would be allowed to escape the hardbanding surface.
On the other hand, it should be mentioned that an increase in test duration may affect the shear history of the mud to such extent that its lubricating properties change significantly. In addition, longer test duration means more accumulated wear debris, thus also abrasive particles. To prevent these potential effects it can be used a larger mud volume, or circulate the mud during testing.

9.6 Pin weight loss and the performance of hardbanding materials

Even though the main objective of this master thesis was to reproduce the wear mechanisms from the full-scale tests, a lot of information about the different hardbanding materials have been collected throughout the experimental process and is worth mentioning.

Behind the wear mechanisms and the many parameters such as sand content, contact pressures and mud viscosity, the most important result for the industry is how fast the materials are worn out. A comparison of the pin weight loss of the five different hardbanding materials are shown in figure 45. It is easily seen that the increase in contact pressure from program 1 to program 2 and 3 had major impact

on the wear rate (supporting the theory of a shift from abrasive to adhesive wear regime mentioned earlier). It must be remembered that program 1 had twice the duration of program 2 and 3, and still caused the least amount of pin weight loss. The data from program 2 and 3 are more challenging to interpret as it is more scattered. However, a trend is that program 3 has created less pin weight loss than program 2, with the exception of HB D. This may be caused by the smaller contact area (reduced pin radius) or the increase in sand content.

Amongst the hardbanding materials tested, sample A, B and E showed the least amount of weight loss in all three programs (see figure 45). These samples are also the ones with the highest bulk hardness (especially B and E), while sample C and D with the lowest hardness showed the largest pin weight loss.

Another interesting observation is the difference between pin weight loss of sample B and C, which the latter is essentially a lean (or low) alloyed version of the former. It is thus interesting to see that sample C had a significantly higher wear rate than sample B, with a hardness difference of 150 Vickers as the major disparity. However, since this master thesis only allowed for one repetition to be made, it would be wrongful to draw any conclusions on this topic. Test repetitions are highly recommended in future test programs.

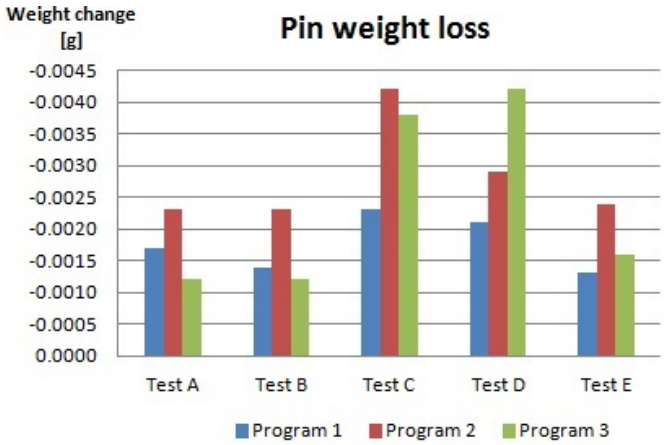

Figure 45: Comparison of pin weight loss.

10 Conclusions

10.1 Wear mechanisms

The lab-scale pin-on-ring test setup was able to reproduce many of the wear mechanisms observed in the full-scale setup.

Adhesive wear by galling, which is regarded as the most important wear mechanism with respect to wear rate, was present in the samples from test program 2 and 3. The casing samples displayed work-hardened layers that contained voids and particles from the hardbanding counterparts. A work-hardened layer was also found on the worn hardbanding samples, but with lesser thickness than in the casing samples.

Abrasive wear was most prominent in test program 1, possibly by the absence of severe damage by adhesion due to insufficient contact pressure. Abrasive wear pattern was also visible on the samples from program 2 and 3, but in much lesser extent compared to the damage created by adhesion.

Fatigue wear in the form of cracking and spalling of the surfaces was only present in the most brittle hardbanding material, and to a very limited extent. It can be concluded that the test duration of 15 minutes was too short for cracking to initiate and propagate, which eventually could have created spalling particles.

10.2 Test parameters

Contact pressure can be concluded to have the largest impact on type of wear and wear rate in these experiments. At low contact pressure in program 1, abrasive wear was prominent, while higher contact pressures in program 2 and 3 promoted adhesive wear.

Regarding the effect of sand it is not possible to draw any conclusions since these experiments do not provide a systematic approach to its effect.

Longer test duration would probably allowed more work-hardening of the contacting surfaces and enhanced the extent of fatigue wear.

11 Further work

Any future work with this lab-scale setup should include the following:

- Validation of the results from these experiments by the use of more test parallels.
- Experiments with longer test duration in order to investigate the development of fatigue wear (cracking and spalling), especially in the hardbanding materials. A larger test tube or a system for circulating the slurry should in that case be considered in order to prevent accumulated wear debris in the system.
- Isolation of the different test parameters such as contact pressure and sand content would provide insight to their separate effect on wear mechanisms and wear rate.

References

[1] Øystein Høgsand. Hardbanding for Ultra-low Friction in Drilling: A Tribological Study. Specialization project NTNU, 2012.

[2] Alvaro Chan et.al. Evolution of Drilling Programs and Complex Well Profiles Drive Development of Fourth-Generation Hardband Technology. Society of Petroleum Engineers, 2008.

[3] G. Robello Azar, J. J. Samuel. *Drilling Engineering*. PennWell, 2007.

[4] K.A. Macdonald and J.V. Bjune. Failure Analysis of Drillstrings. *Engineering Failure Analysis*, 14(8):1641 – 1666, 2007.

[5] Jiangsu Top Drilling Tools. http://toppump.en.ecplaza.net/9.jpg. Image from website.

[6] Steven Ripman. Casing Wear in Multilateral Wells. Master's thesis, University of Stavanger, 2011.

[7] Schlumberger. Schlumberger Oilfield Glossary: Casing Grade. http://www.glossary.oilfield.slb.com/en/Terms/c/casing_grade.aspx, 2013.

[8] Steve Cart. Composition of drilling fluids comprising Ground Elastomeric Crumb Rubber Material and a Method of Decreasing Seepage and Whole Mud Loss Using such Composition. http://www.freepatentsonline.com/6806232.html, October 2004. US patent number: 6806232.

[9] Petroleumstilsynet. Deepwater Horizon-ulykken - Vurderinger og anbefalinger for norsk petroleumsvirksomhet. Report, Petroleumstilsynet, 2011.

[10] John G. Mobley. Hardbanding and its Role in Deepwater Drilling. Society of Petroleum Engineers, 1999.

[11] Schlumberger. Schlumberger Oilfield Glossary: Dogleg. http://www.glossary.oilfield.slb.com/en/Terms/d/dogleg.aspx, 2013.

[12] Schlumberger. Schlumberger Oilfield Gloassary: Key Seat. http://www.glossary.oilfield.slb.com/en/Terms.aspx?LookIn=term2013.

[13] M. Mims. *Drilling Design and Implementation for Extended Reach and Complex Wells*. K & M Technology Group, 2002.

[14] Society of Petroleum Engineers. Mud Related Drilling Problems Differential Sticking. http://pet-oil.blogspot.no/2010/07/mud-related-drilling-problems.html, 2010. SPE.

[15] Schlumberger. Schlumberger Oilfield Glossary: Directional Drilling. http://www.glossary.oilfield.slb.com/en/Terms/d/directional_drilling.aspx, 2013.

[16] Katie Mazerov. Harsh Environments, Extended Drilling Envelopes Steer Drill pipe Evolution. http://www.drillingcontractor.org/harsh-environments-extended-drilling-envelopes-steer-drill-pipe-evolution-21261, 2013. Drilling Contractor.

[17] John G. Mobley. Finally, the Truth About Drill String Hardbanding. *Drilling Contractor*, 2007.

[18] Bruno Best. Casing Wear Caused by Tooljoint Hardfacing. *SPE Drilling Engineering*, February 1986.

[19] Joe Haberer. New Solutions May Ease Hardbanding Controversy. *Drilling Contractor*, 2000.

[20] Trio OilTec Services. Hardbanding for Oil and Gas Drilling. http://www.otw-hardbanding.com, 2013. Printed booklet and web.

[21] SR-Services. Hardbanding. http://www.srservices.org/hardbanding.php, 2013. Webpage.

[22] John J. Truhan, Ravi Menon, and Peter J. Blau. The Evaluation of Various Cladding Materials for Down-Hole Drilling Applications Using the Pin-On-Disk Test. *Wear*, 259(7–12):1308–1313, 2005. 15th International Conference on Wear of Materials.

[23] John Truhan, Ravi Menon, Frank LeClaire, Jack Wallin, Jun Qu, and Peter Blau. The Friction and Wear of Various Hard-Face Claddings for Deep-Hole Drilling. *Wear*, 263(1–6):234 – 239, 2007. 16th International Conference on Wear of Materials.

[24] Martin True and Peter Weiner. Optimum Means of Protecting Casing and Drillpipe Tool Joints Against Wear. *Journal of Petroleum Technology*, 1975.

[25] Schlumberger. Schlumberger Oilfield Gloassary: Casing. http://www.glossary.oilfield.slb.com/en/Terms/c/casing.aspx, 2013.

[26] Jerry White and Rapier Dawson. Casing Wear: Laboratory Measurements and Field Predictions. *SPE Drilling Engineering*, 1987.

[27] ISO. *ISO 11960, Petroleum and Natural Gas Industries – Steel Pipes for Use as Casing or Tubing for Wells*, 2011. Table E.3.

[28] Ernest Rabinowicz. *Friction and Wear of Materials*. John Wiley and Sons, Inc., 1995.

[29] Gwidon W. Stachowiak and Andrew W. Batchelor. *Engineering Tribology*. 2006.

[30] A. R. Doering, D. R. Danks, S. E. Mahmoud, and J. L. Scott. Evaluation of Worn Tubulars from DEA-42 and Small-Scale Casing Wear Testers. 2011.

[31] ASTM International. *G40-12: Standard Terminology Relating to Wear and Erosion*, 2012.

[32] I.M Hutchings. *Tribology: Friction and Wear of Engineering Materials*. Butterworth-Heinemann, 1992.

[33] Lars Lunde. Wear, Tribology and Coating Technology. Lecture, 2012.

[34] G. M. Erlikh, N. A. Vartanova, and E. I. Revitskii. A New Method of Designing Casing Strings to Withstand Wear due to Friction. *Neft. Khoz*, 1962.

[35] William B. Bradley. Experimental Determination of Casing Wear by Drill String Rotation. *Journal of Engineering for Industry*, 1975.

[36] William B. Bradley and John E. Fontenot. The Prediction and Control of Casing Wear. *Journal of Petroleum Technology*, 1975.

[37] J. Steve Williamson. Casing Wear: The Effect of Contact Pressure. *Journal of Petroleum Technology*, 1981.

[38] Ali Y. Garkasi, Yanghua Xiang, and Gefei Liu. Casing Wear in Extended Reach and Multilateral Wells. http://www.worldoil.com/Casing-wear-in-extended-reach-and-multilateral-wells.html, 2010.

[39] Robert W. Bruce. *Handbook of Lubrication and Tribology*. CRC Press, 2 edition, 2012.

[40] Johan Pettersen. *Overall Evaluation of Offshore Drilling Fluid Technology: Development and Application of Life-cycle Inventory and Impact Assessment Methods*. Phd. thesis, Norwegian University of Science and Technology, Department of Energy and Process Engineering, 2007. Doktoravhandlinger ved NTNU.

[41] B.J. Briscoe, P.M. Cann, A. Delfino, and G. Maitland. Lubrication of Water-Based Clay Suspensions. *Tribology Research: From Model Experiment to Industrial Problem*, pages 331–340, 2001.

[42] G.M. Bol. Effect of Mud Composition on Wear and Friction of Casing and Tool Joints. *SPE Drilling Engineering*, pages 369–376, 1986.

[43] J.F. Archard. Contact and Rubbing of Flat Surfaces. *Applied Physics*, 24:981–990, 1953.

[44] R.W Hall and K.P Malloy. Contact Pressure Threshold: An Important New Aspect of Casing Wear. *SPE*, 2005.

[45] R.W Hall, Ali Garkasi, Greg Deskins, and John Vozniak. Recent Advances in Casing Wear Technology. *SPE*, 1994.

[46] A.A. Torrance. Modelling Abrasive Wear. *Wear*, 258(1–4):281 – 293, 2005. Second International Conference on Erosive and Abrasive Wear.

[47] Jorunn Øvsthus. E-mail correspondance. E-mail, May 2013. E-mail correspondance with assistant laboratory manager at Mi Swaco, supplier of drilling mud systems.

A Typical welding parameters for Hardbanding application

Table 19: Typical welding parameters of hardbanding materials. Provided by Trio Oiltec Services.

Process	GMAW (automatic)
Electrode size	1,6 mm
Shielding gas	Type (M21) 75Ar/25CO_2 or 82Ar/18CO_2 to 97,5Ar/2,5CO_2 (M12) Also pure CO_2 (C1) can be used.
Pre-heat	According to base metal, suggested: $>$ 25 mm 180 - 260°C $<$ 25 mm 93 - 180°C
Current type/Polarity	DC (+) DCEP
Amperage	220 - 280 A
Voltage	24 - 30 V
Interpass temperature	Max 450°C
Cooling	Slow cool

B Complete Hertzian equations

Reduced Young's modulus:

$$\frac{1}{E'} = 1/2 \left[\frac{1-\nu_A^2}{E_A} + \frac{1-\nu_B^2}{E_B} \right] \tag{10}$$

Reduced radius of curvature for contact between two bodies a and b:

$$\frac{1}{R_x} = \frac{1}{R_{ax}} + \frac{1}{R_{bx}} \tag{11}$$

$$\frac{1}{R_y} = \frac{1}{R_{ay}} + \frac{1}{R_{by}} \tag{12}$$

$$\frac{1}{R'} = \frac{1}{R_x} + \frac{1}{R_y} \tag{13}$$

Elliptic contact area dimensions:

$$a = k_1 \left(\frac{3WR'}{E'} \right)^{1/3} \tag{14}$$

$$b = k_2 \left(\frac{3WR'}{E'} \right)^{1/3} \tag{15}$$

Maximum contact pressure:

$$p_{max} = \frac{3W}{2\pi ab} \tag{16}$$

Mean contact pressure:

$$p_{mean} = \frac{W}{\pi ab} \tag{17}$$

C Worn samples from the test programs

C.1 Full-scale samples

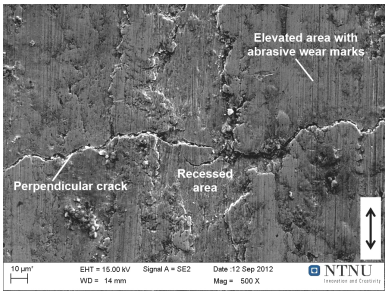

(a) Hardbanding A surface,500X.

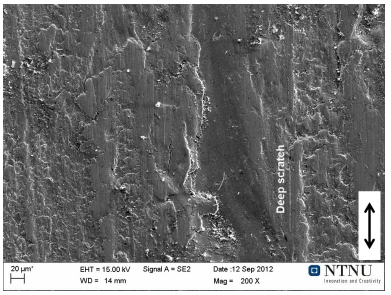

(b) Casing A surface, 200X.

Figure 46: Worn surfaces on HB/casing A from full-scale tests.

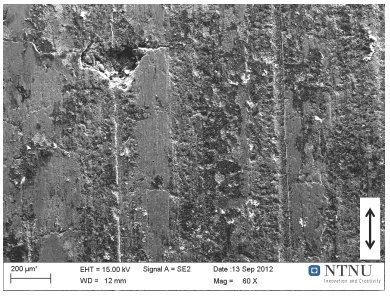

(a) Hardbanding B surface, 60X.

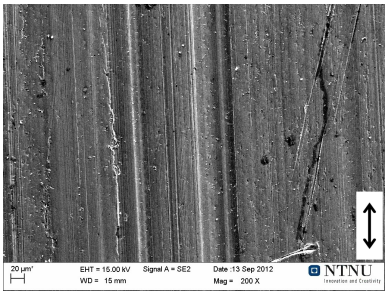

(b) Casing B surface, 200X.

Figure 47: Worn surfaces on HB/casing B from full-scale tests.

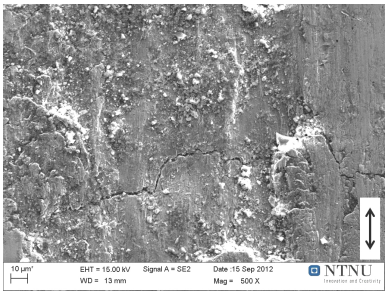

(a) Hardbanding C surface, 500X.

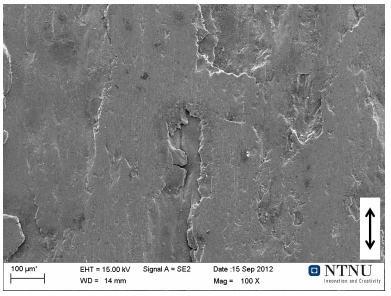

(b) Casing C surface, 100X.

Figure 48: Worn surfaces on HB/casing C from full-scale tests.

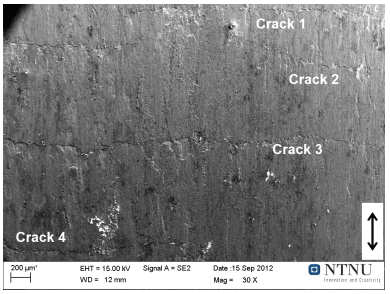

(a) Hardbanding D surface, 30X.

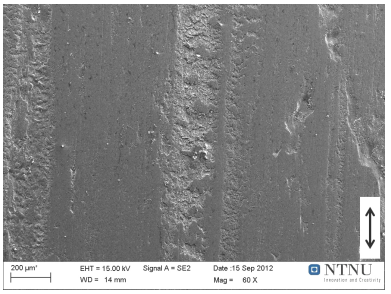

(b) Casing D surface, 60X.

Figure 49: Worn surfaces on HB/casing D from full-scale tests.

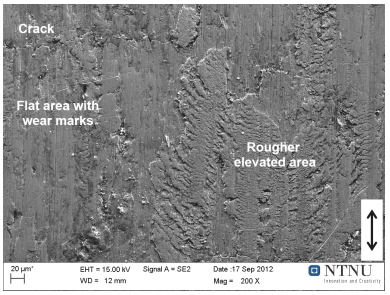

(a) Hardbanding E surface, 200X.

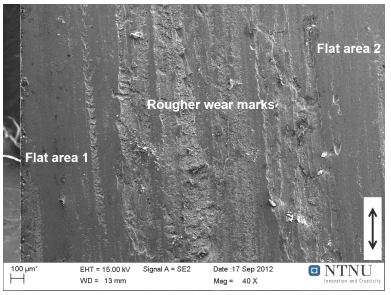

(b) Casing E surface, 40X.

Figure 50: Worn surfaces on HB/casing E from full-scale tests.

C.2 Program 1 samples

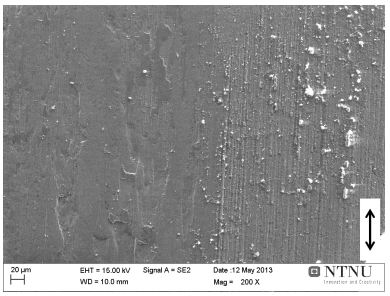

(a) Hardbanding A surface, 200X.

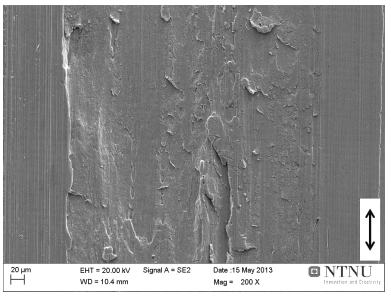

(b) Casing A surface, 200X.

Figure 51: Worn surfaces on HB/casing A from program 1.

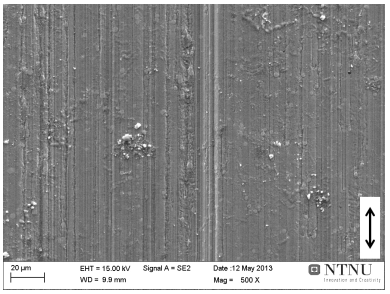

(a) Hardbanding B surface, 500X.

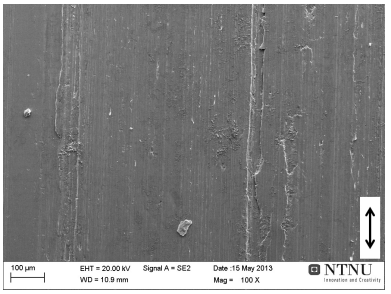

(b) Casing B surface, 100X.

Figure 52: Worn surfaces on HB/casing B from program 1.

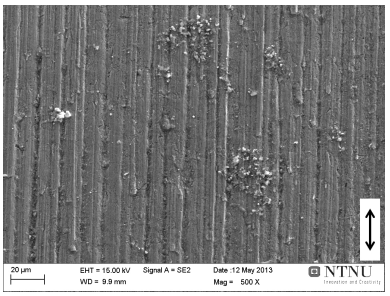

(a) Hardbanding C surface, 500X.

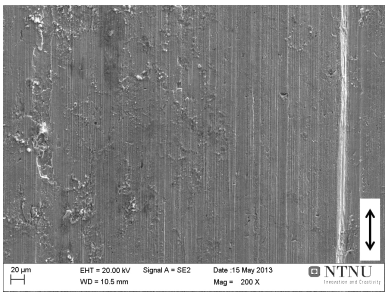

(b) Casing C surface, 200X.

Figure 53: Worn surfaces on HB/casing C from program 1.

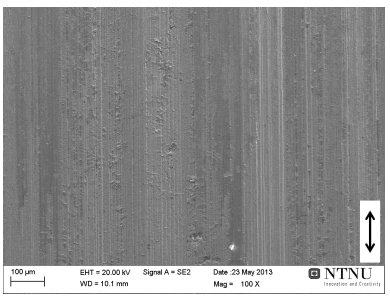

(a) Hardbanding D surface, 100X.

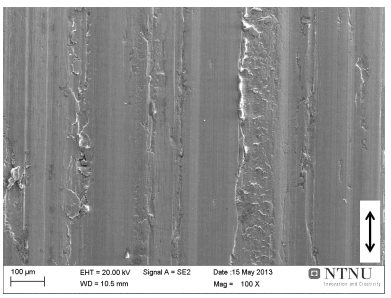

(b) Casing D surface, 100X.

Figure 54: Worn surfaces on HB/casing D from program 1.

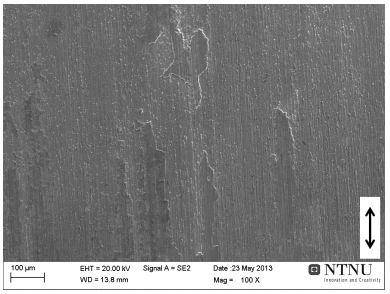

(a) Hardbanding E surface, 100X.

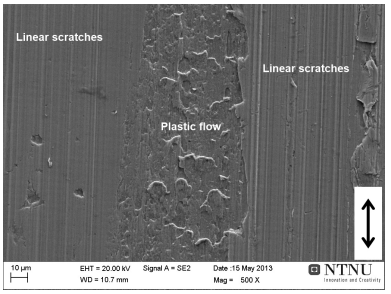

(b) Casing E surface, 500X.

Figure 55: Worn surfaces on HB/casing E from program 1.

C.3 Program 2 samples

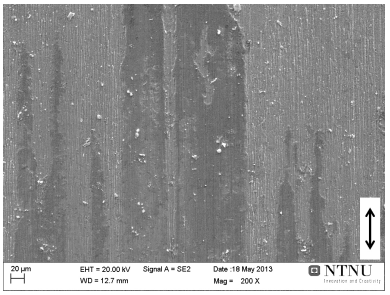

(a) Hardbanding A surface, 200X.

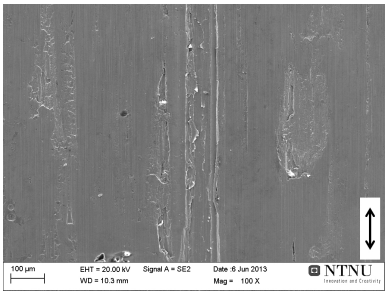

(b) Casing A surface, 100X.

Figure 56: Worn surfaces on HB/casing A from program 2.

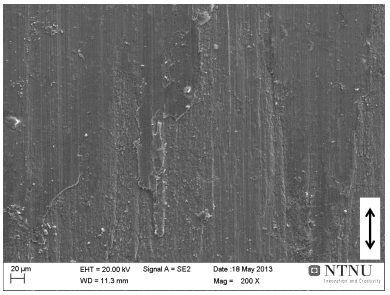

(a) Hardbanding B surface, 200X.

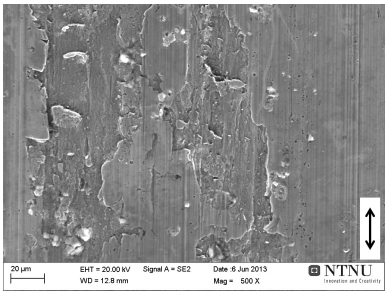

(b) Casing B surface, 500X.

Figure 57: Worn surfaces on HB/casing B from program 2.

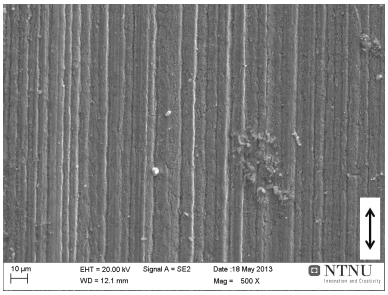

(a) Hardbanding C surface, 500X.

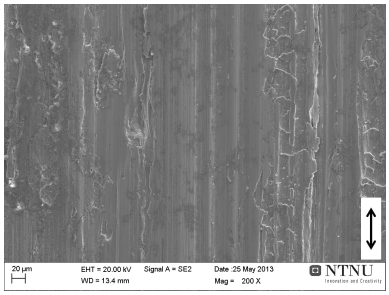

(b) Casing C surface, 200X.

Figure 58: Worn surfaces on HB/casing C from program 2.

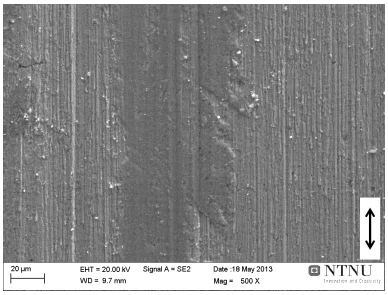

(a) Hardbanding D surface, 500X.

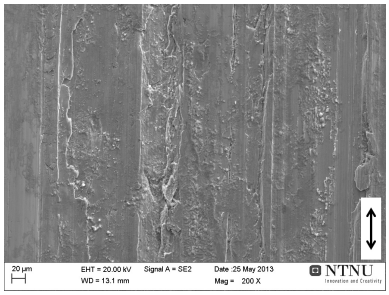

(b) Casing D surface, 200X.

Figure 59: Worn surfaces on HB/casing D from program 2.

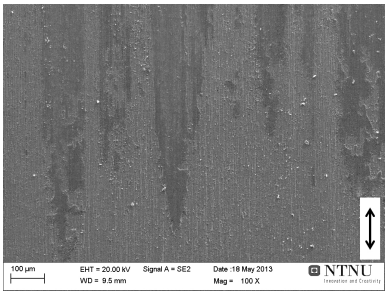

(a) Hardbanding E surface, 100X.

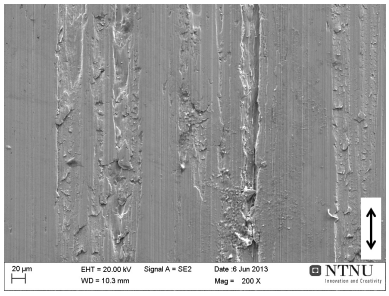

(b) Casing E surface, 200X.

Figure 60: Worn surfaces on HB/casing E from program 2.

C.4 Program 3 samples

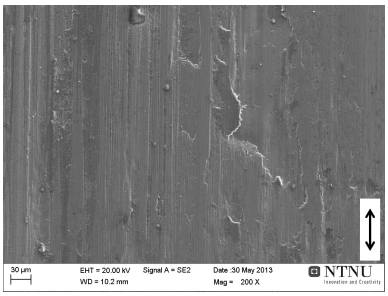

(a) Hardbanding A surface, 200X.

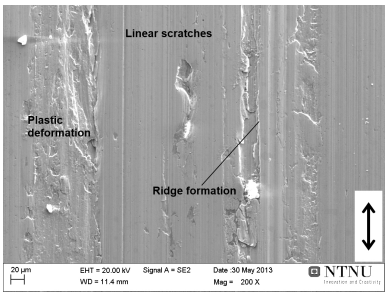

(b) Casing A surface, 200X.

Figure 61: Worn surfaces on HB/casing A from program 3.

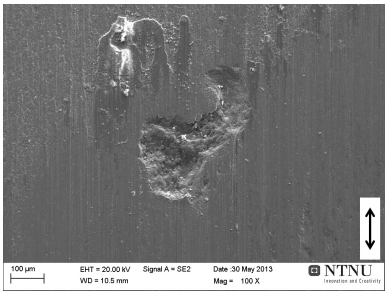

(a) Hardbanding B surface, 100X.

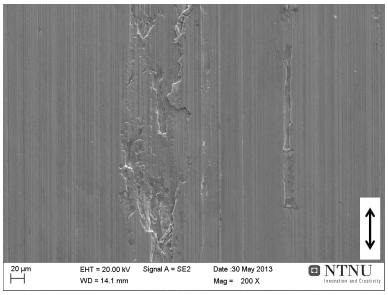

(b) Casing B surface, 200X.

Figure 62: Worn surfaces on HB/casing B from program 3.

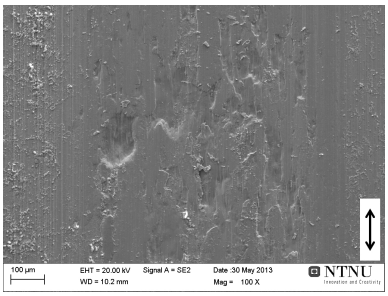

(a) Hardbanding C surface, 100X.

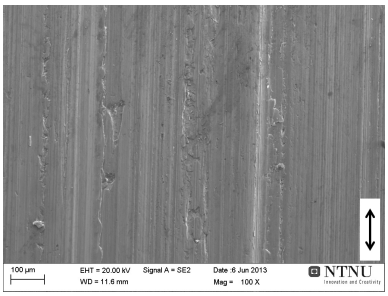

(b) Casing C surface, 100X.

Figure 63: Worn surfaces on HB/casing C from program 3.

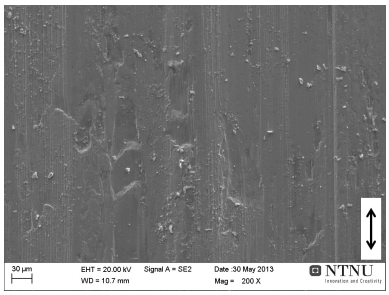

(a) Hardbanding D surface, 200X.

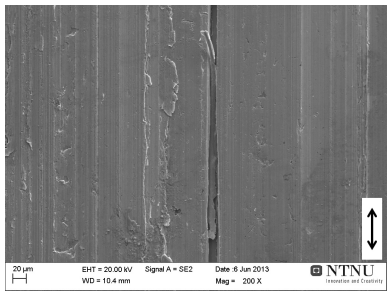

(b) Casing D surface, 200X.

Figure 64: Worn surfaces on HB/casing D from program 3.

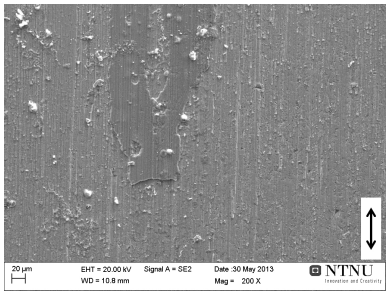

(a) Hardbanding E surface, 200X.

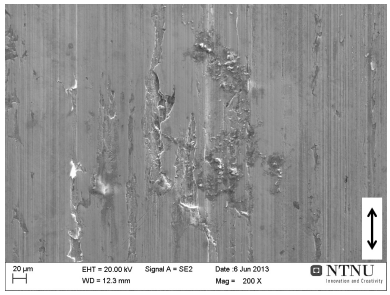

(b) Casing E surface, 200X.

Figure 65: Worn surfaces on HB/casing E from program 3.

C.5 Additional images

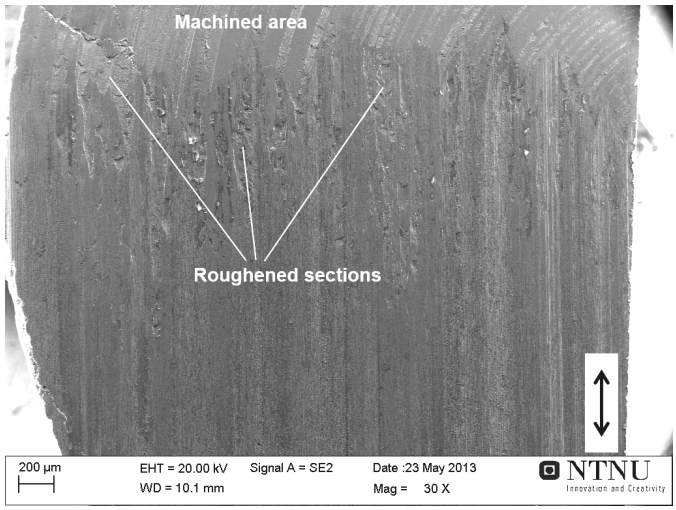

Figure 66: Overview of worn hardbanding from program 1. HB D, 30X.

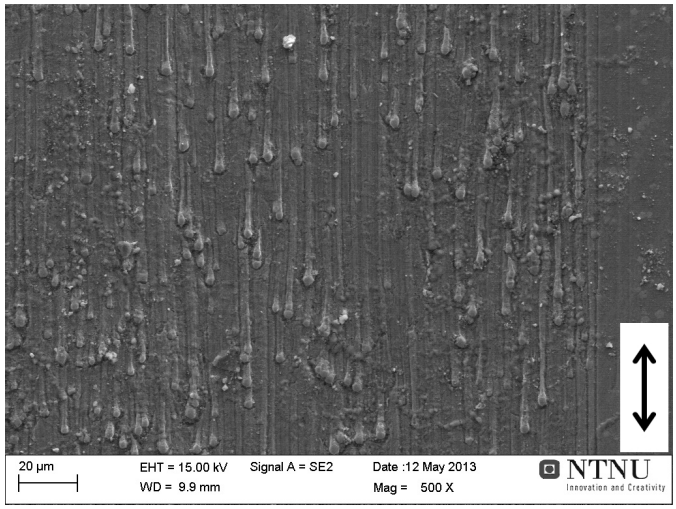

Figure 67: Tear-drop pattern formed by the dragging of hardbanding particles in program 1. HB B, 500X.

D EDS spectra

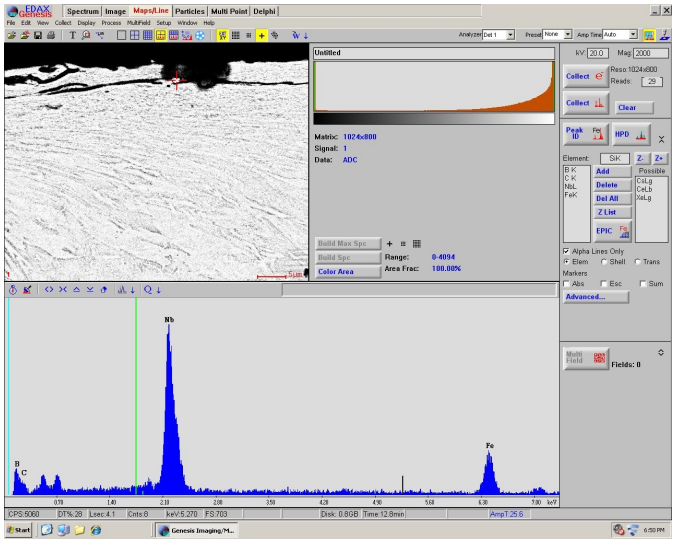

Figure 68: EDS analysis of particle found in deformed surface layer in casing B from test program 2.

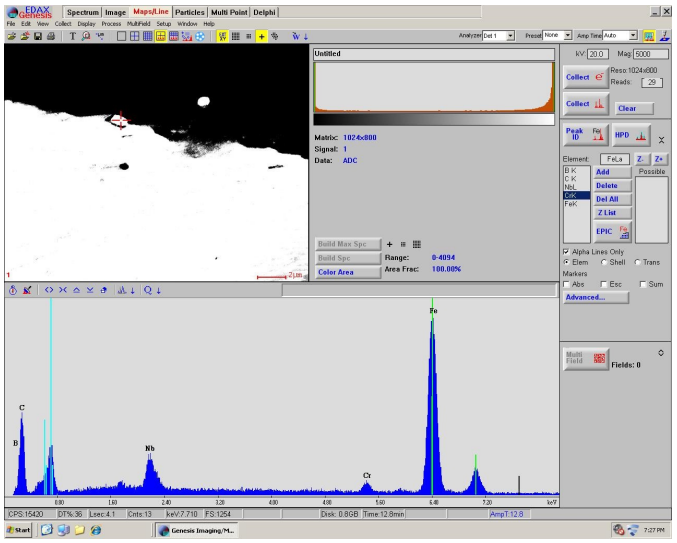

Figure 69: EDS analysis of particle found in deformed surface layer in casing E from test program 2.